Opa1 helical structures give perspective to mitochondrial dysfunction

Jenny Hinshaw (jennyh@niddk.nih.gov)
National Institutes of Health

Sarah Nyenhuis
Laboratory of Cell and Molecular Biology, National Institute of Diabetes and Digestive and Kidney Diseases, National Institutes of Health

Xufeng Wu
NHLBI Light Microscopy Facility, National Institutes of Health

Abigail Stanton
NIH

Marie-Paule Strub
National Heart, Lung and Blood Institute

Yang-In Yim
NIH

Bertram Canagarajah
NIH

Biological Sciences - Article

Keywords:

Posted Date: September 14th, 2022

DOI: https://doi.org/10.21203/rs.3.rs-2039298/v1

Opa1 helical structures give perspective to mitochondrial dysfunction

Sarah B. Nyenhuis[1], Xufeng Wu[2], Abigail E. Stanton[1,3], Marie-Paule Strub[4], Yang-In Yim[5], Bertram Canagarajah[1], & Jenny E. Hinshaw[1*]

[1]Laboratory of Cell and Molecular Biology, National Institute of Diabetes and Digestive and Kidney Diseases, NIH, Bethesda, MD, USA.
[2]Light Microscopy Facility, National Heart, Lung, and Blood Institute, NIH, Bethesda, MD, USA.
[3]Currently, Molecular Biology Department, Princeton University, Princeton, NJ, USA.
[4]Protein Expression Facility, National Heart, Lung, and Blood Institute, NIH, Bethesda, MD, USA.
[5]Cell and Developmental Biology Center, National Heart, Lung and Blood Institute, NIH, Bethesda, MD, USA.
[*]e-mail: jennyh@niddk.nih.gov

Abstract

Dominant Optic Atrophy is the leading cause of childhood blindness, with 60-80% of cases caused by mutation of the gene encoding the protein Optic Atrophy 1, OPA1. This condition dysregulates the GTPase mediated fusion process of the mitochondrial inner- and outer-membranes. OPA1 is critical to the dynamic organization and regulation of the mitochondria due to its role in cristae remodeling and GTPase-mediated fusion of the inner mitochondrial membrane. Here, we solved helical structures of OPA1 assembled on lipid membrane tubes, in the presence and absence of nucleotide by cryo-electron microscopy methods. These helical assemblies organize into densely packed protein rungs with minimal inter-rung connectivity and exhibit nucleotide-dependent dimerization of the GTPase domains, a hallmark of dynamin superfamily proteins (DSPs). In contrast to other DSPs, OPA1 contains several unique secondary structures in the paddle domain that strengthen its membrane association. The novel structural features identified in this study shed light on the effects of pathogenic point mutations on protein folding, inter-protein assembly, and membrane interactions. Further, mutations chosen to disrupt OPA1 assembly interfaces and membrane binding cause mitochondrial fragmentation in cell-based assays, demonstrating the biological relevance of these interactions.

Main

Mitochondria are doubly-enveloped organelles with the inner mitochondrial membranes (IMM) marked by frequent invaginations or cristae[1-3]. Membrane fusion and fission processes of the double membrane, driven by dynamin superfamily proteins (DSPs), are critical to the dynamic organization and regulation of mitochondria[1,2,4]. For the outer mitochondrial membrane (OMM), mitofusins 1 and 2 (Mfn1/2) and dynamin-related protein (DRP1) mediate fusion and fission, respectively[2,5-10]. In the IMM, Optic Atrophy 1 (OPA1) mediates membrane fusion, cristae remodeling, mitochondrial DNA maintenance, and potentially membrane fission (Fig. 1a)[2,11-13]. OPA1 exists in two forms *in vivo*: the long-form is tethered to the IMM through a single transmembrane domain, which is proteolytically cleaved in the inner membrane space (IMS) to yield the short form (sOPA1)[1, 12, 23].

The OPA1 gene is the most frequently mutated gene in the disease Dominant Optic Atrophy (DOA), the leading cause of childhood blindness, which results from progressive degeneration of retinal ganglion cells[14-18]. According to the LOVD database, there are currently over 640 unique mutations identified in the OPA1 gene[14]. Confirmed or suspected pathogenic mutations of OPA1 cause a wide array of phenotypic symptoms: progressive vision loss, hearing loss, ataxia, and myopathy[14-18]. On the molecular level this is caused by mitochondrial dysfunction, including: fragmentation of the mitochondrial network, mitochondrial-DNA loss, and loss of overall respiratory function[13,15,18]. The urgency to develop a treatment for DOA has led to significant interest in OPA1, yet the mechanics of its roles in membrane remodeling remain elusive[2,12,13,19]. Previous structural studies on OPA1 or its yeast ortholog, MGM1, have suggested similarities between OPA1 and other DSPs, but the insight of these studies on pathological OPA1 mutations has been limited by a lack of context of the full construct, a membranous environment, or the freedom to form higher-order assemblies[20,21]. In addition, the presence of varied OPA1 isoforms and the diversity of its mitochondrial roles suggests further complexity to the connection between OPA1 structure and disease.

There are eight OPA1 isoforms, all of which contain an S1 cleavage site within the N-terminal domain for the protease OMA1 in response to membrane depolarization. Four isoforms contain a second S2 cleavage site for YME1L, which is coupled to the respiratory state of the mitochondria (Supplementary Fig. 1) [12,13,22], while isoform 5 contains a third YME1L cleavage site[23]. These cleavage events result in a dynamic ratio of the long and short forms of OPA1 to regulate mitochondrial morphology and function[12,13,24]. During the fusion event, OPA1 must bring together or tether two IMM leaflets from distinct mitochondria[1,13,24]. This is likely followed by the formation of a higher order assembly, such as a helical bundle, surrounding the membrane surface[18,21]. A final conformational change, such as the mechanochemical powerstroke seen for other DSPs, would then lead to the fusion event[25,26]. OPA1 may use a similar mechanism to regulate cristae structure[2,20].

Structurally, there are two available X-ray structures of soluble OPA1 orthologs, MGM1 from *C. thermophilum* and *S. cerevisiae*, that reveal the overall architecture of short MGM1[20,27] The *C. thermophilum* X-ray structure has a similar tetrameric organization to other DSPs and docking the structure into cryo-electron tomograms also showed similar protein:protein interfaces (PDB: 6QL4)[20,28]. However, unlike other DSPs, nucleotide dependent dimerization of the MGM1 GTPase domains was not observed[20]. The *S. cerevisiae* MGM1 structure captured the short form of MGM1 as a trimer in the presence of guanosine diphosphate (GDP) (PDBID: 6JSJ), which revealed a novel GTPase:membrane interaction[27]. These studies advanced the structural information available for IMM fusion, but the low ~30% sequence identity of MGM1 to OPA1 hinders their ability to inform on human pathologies associated with DOA[20,27]. There are also low-resolution cryo-electron microscopy (cryoEM) structures of MGM1 and OPA1 as helical assemblies[20,21]. Curiously, the MGM1 helix assembled on both the outside and inside of the lipid tube[20], where the inner helical lattice presents a possible mechanism for cristae remodeling (PDB ID: 6RZV, 6RZW)[20]. The outer MGM1 and OPA1 helical assemblies were solved for two states (Apo and GTPgS) at relatively low resolutions (~15-23 Å). Surprisingly, no GTPase domain dimerization was observed in either structure in the presence of GTPgS[24,20], although a nucleotide dependent GTPase domain dimer was observed for a short construct consisting of just the GTPase and BSE region (PDBID: 6JTG)[29]. This dimer interface is similar to other DSP structures, but the result was still isolated from the whole sOPA1 construct, membrane environment, or helical assembly[29].

Here, we present two cryoEM structures of human sOPA1 assembled on a cardiolipin containing lipid bilayer (DOPS:CL, 75:25) in the absence and presence of nucleotide (GDP-AlF_x) (Fig. 1c-e and Extended Data Fig. 1). The full helical maps resolved to 5.48 Å in the presence of nucleotide and 9.68 Å in its absence (Fig. 1c-e). Z-clipping to 50% of the full map improved the resolutions to 3.86 Å and 5.8 Å, respectively (Extended Data Fig. 1c-f). We then further improved the resolution using local non-uniform refinements (see workflow in Supplementary Figs. 2, 3)[30,31] to 3.1-6.5 Å, from which we were able to build models of sOPA1 (Fig. 1c and Extended Data Fig. 2, 3). The observed domain organization of the sOPA1 monomer parallels other DSPs, with GTPase, BSE, and stalk domains (Fig. 1b,c)[2, 28, 29]. In contrast to other DSPs, however, sOPA1 has a uniquely kinked stalk[20], an N-terminal coiled-coil juxta-membrane linker, and a cardiolipin specific paddle domain[18,32](Fig. 1c). Using this model, we could locate DOA-associated point mutations and hypothesize how clinically significant mutations disrupt OPA1 function (Fig. 1c and Extended Data Table 1).

The sOPA1 assemblies with and without nucleotide are 38.2 nm and 40.5 nm in diameter, respectively (Fig. 1d,e left side and Extended Data Fig. 1a,b), where both are narrower than previously observed structures[20,21]. This is likely due to the nucleotide state (transition state, GDP-AlF_x, versus GTP bound state, GTPγS). From these structures we were able to define novel oligomeric and membrane binding interfaces, identify the canonical nucleotide-dependent dimerization of the GTPase domains, and observe a new inter-rung N-terminal coiled-coil interface (Figs. 1d,e, 2). While the sOPA1 maps still possess substantial flexibility due to minimal inter-rung connectivity, as evidenced by the inherent curvature of the sOPA1 tubes, they also display dense intra-rung packing (Supplementary Fig. 2a). This dense protein network, together with the reduced diameter and higher resolution suggests the two structures presented here are stable intermediates in the later stages of the energy landscape of the fusion pathway.

Local refinements also improved the resolution of novel interfaces that define the oligomerization of sOPA1. The building block of sOPA1 helical assemblies is a dimer, which is defined by 3 interfaces (interfaces 1-3) (Fig. 1d and Extended Data Figs. 2, 3a). Further assembly of OPA1 is driven by dimer-dimer assembly into tetramers through a paddle:paddle contact, interface-4, with additional contributions from two smaller interfaces near the GTPase domain (interface-6 and -9) (Figs. 1e, 2a,c,f and Extended Data Fig. 3b,d,g). Additional dimers assemble on both sides of a tetramer, through interfaces 4, 6 and 9, to generate a helical rung. In the nucleotide-bound state, the helical assembly is further stabilized by the GTPase domain dimer (interface-5) along the biological rung (Fig. 2b, Supplementary Fig. 3h, Extended Data Fig. 3c). Finally, two inter-rung contacts involve the paddle (interface-7) and N-terminal (interface-8) domains (Fig. 2d,e and Extended Data Fig. 3e,f), further stabilizing sOPA1's oligomerization.

Though the overall shape of the sOPA1 assembly is similar to other DSPs, the defining interfaces are unique. The stalk-dimer interface (interface-1) occurs along the opposite face of the stalk's 4-helix bundle compared to MGM1[20]. This results in a more compressed and extensive "W"-shape interface due to the tightly interlocked nature of the kinked-stalk (interface-1 in Fig. 1d,e and Extended Data Fig. 2a,d). Because of interface-1's position within the sOPA1 GDP-AlF_x dimer, the buried surface area between stalk and paddle domains extends into several other regions (Extended Data Fig. 2a, middle). The entire buried surface area of a dimeric unit of sOPA1 with GDP-AlF_x bound covers an average area of 1429 $Å^2$ (Extended Data Fig. 2a, middle and Supplementary Table 1)[33], 18% more than in MGM1[20]. The dimer is further stabilized by two additional interfaces, one between the stalk and paddle (interface-2) and another between the Pα5 helices in the paddle domain (interface-3) (Fig. 1d, Extended Data Figs. 2a,d, 6a and

Supplementary Table 1)[33]. Further assembly into a tetramer is driven by linking the paddle-hinges of two dimers near the membrane surface (interface-4), involving Pα1 and Pα6 (Figs. 1e, 2a, Extended Data Fig. 2a,d and Supplementary Data Table 1). In the GDP-AlF_x state, we also resolved two smaller interfaces (interface-6, and interface-9) that further stabilize the tetramer (Fig. 2c,f and Extended Data Fig. 3d,g).

Upon nucleotide binding, the helical assembly of sOPA1 undergoes a large conformational change resulting in a more compact, organized assembly due to dimerization of the GTPase domain (Supplemental Movie 1). The GTPase dimer interface (interface-5), also known as the G2 interface[32], is by far the largest interface in the sOPA1 oligomer and resides within a helical rung, whereas in other DSPs the G2 is between rungs (Fig. 2b, Supplementary Fig. 3h, Extended Data Fig. 3c). To dimerize, the GTPase domain and BSE must swing 25-27° upon GDP-AlF_x binding (Fig. 3a,b). The GTPase interface and nucleotide binding pocket resemble the crystal structure of the minimal OPA1 GTPase domain dimer bound to GDP-BeF_x (PDB ID: 6JTG, RMSD=2.995 Å), but with increased asymmetry along the dimer interface (Extended Data Fig. 4a-b)[29,39]. Incorporation into the helical assembly also results in a small swing of the BSE region, which is less resolved, likely due to heterogeneity or pull from the N-terminal region. Consistent with this, mapping the per-particle heterogeneity of both assemblies in cryoDRGN showed continuous transitions within the N-terminal and GTPase dimer regions (Supplementary Fig. 3r-t and Movie 2)[31]. Relative to the crystal structure, the BSE helices of the GDP-AlF_x bound assembly are offset 30.31° in the A-chain and 22.26° in the B-chain (Extended Data Fig. 4b). These shifts in the BSE suggest potential energy is stored in the sOPA1 assembled state to assist in eventual disassembly, a step that may be required for membrane fusion.

Previous structural studies of dynamin observed a large swing of the BSE during the GTPase hydrolysis cycle referred to as the powerstroke[34]. In the proposed powerstroke, the BSE is in the up position in the GTP bound state and swings down upon hydrolysis (Extended Data Fig. 4c)[34]. The positioning of the sOPA1 BSE, relative to the GTPase domain, is in the down position, similar to dynamin in the presence of GDP-AlF_x[35]. Curiously, the positioning of the BSE in pre-powerstroke or up position has not been observed for OPA1 or MGM1, even in the presence of GTPgS, a GTP-bound state[20,21].

In the paddle domain, interface-7 provides one of the few inter-rung contacts in the helical assemblies through Pα4 (Fig. 2d and Extended Data Figs. 2a,d, 3e), with similar buried surface area in the two states (Supplementary Table 1)[33]. Strikingly, in the GDP-AlF_x bound state we were also able to resolve a second inter-rung interface (interface-8) that resides above interface-7 and consists of a coiled-coil domain assembled from the N-terminal α-helix, Nα1 (Fig. 2e and Extended Data Fig. 3f). This N-terminal region is unique to homologs of sOPA1 and has not been previously resolved in other OPA1 structures. Additionally, despite its inherent flexibility, we found the N-terminal domain also interacts with the BSE domain (interface-9) (Supplementary Table 1 and Fig. 2e)[33]. While poorly resolved, considering that we still observe electron density for the N-terminal region in the apo state, and this region is known to dimerize in the absence of nucleotide, we expect the N-terminal domain still plays a major role in the apo assembly[21]. Overall, the absence of interfaces and decreased buried surface area in the apo state illustrates sOPA1 is more loosely packed prior to nucleotide addition and correlates with an increased variance in apo state diameters, explaining the apo structure's more limited resolution (Supplementary Table 1 and Supplementary Fig. 2b)[33].

Our sOPA1 structure reveals a unique lipid binding motif in the paddle domain that has evolved over time to include membrane-inserting helices (Pα6 and Pα2) and a pair of helices that

reside proximal to the bilayer (Fig. 3c,d). The paddle domain connects to the stalk domain through hinge-3, which includes a disulfide bond that defines the paddle-hinge (OPA1 residues 856C-874C) (Extended Data Fig. 5b,d). Compared to MGM1, the paddle-hinge of OPA1 is extended by the Pα6 helix that inserts into the membrane, resulting in 3 more positively charged or aromatic residues (Extended Data Fig. 5b,c,d)[20]. Additionally, in the paddle-tip along the opposite surface of the paddle domain, the turn between the Pα1 and Pα3 helices is also extended in OPA1 by a flexible membrane-inserting Pα2 helix, which has 9 additional charged or aromatic residues (Fig. 3b-d and Extended Data Fig. 5c,d). OPA1 also has two central helices, Pα1 and Pα5, which are interfacial with the membrane, and are similar in length to MGM1, but OPA1 has 5 more positively charged residues (Extended Data Fig. 5c,d). Accordingly, this results in the OPA1 paddle being oriented more towards the membrane surface than seen for MGM1. Finally, OPA1 has a Pα4 helix which forms interface-7 with a neighboring paddle domain and is anchored to the membrane through residue 824R (Fig. 2d and Extended Data Fig. 5c). MGM1 may compensate for the lack of the Pα4 helix through the presence of an extended loop projecting out of the stalk, with 5 positively charged or aromatic residues[20]. These differences in paddle composition and structure suggest that the OPA1 paddle has evolved to enhance interactions with the IMM, through an extended paddle domain that can support a higher degree of hydrophobic burial, and which likely has higher affinity for negatively charged lipid head groups than other DSPs.

When comparing the apo and GDP-AlF_x sOPA1 states, the paddle domains are more closely associated to the membrane in the nucleotide bound case, with more insertion of the paddle-tip (Pα2-4) and paddle-hinge (Pα6) helices (Fig. 3a,b). Additionally, the Pα1 and Pα5 helices rest on the membrane surface in the GDP-AlF_x bound case (Fig. 3b, right). In contrast, the paddle of the apo state is less deeply inserted with floating Pα1 and Pα5 helices (Fig. 3b, left). We propose the increased membrane interactions upon nucleotide binding are driven by the GTPase domain dimerization, leading to a more compact structure that pushes the paddle deeper into the underlying membrane.

Notably, electrostatics appear to play a more prominent role in the two sOPA1 assemblies than seen for other DSPs (Extended Data Fig. 6a-f). Putatively, the initial attraction between sOPA1 and the cardiolipin containing membrane is aided both by electrostatic contact and hydrophobic insertion (Extended Data Fig. 6a-l). The Pα1 and Pα5 helices are largely positively charged, which would be interfacial to the negatively charged lipid headgroups of the bilayer (Extended Data Fig. 6b). The hydrophobic (gold), aromatic rich helices (Pα2 and Pα6) would then be stabilized by insertion into the lipid tails of the membrane (Extended Data Fig. 6h). Overall, the OPA1 paddle possesses more propensity for charged and hydrophobic membrane interactions that likely optimizes its IMM affinity (Extended Data Fig. 6).

The interfaces between sOPA1 monomers and dimeric assemblies appear to also have large contributions from aligned electrostatic potential. The sOPA1 dimer is striated in positive and negative charge and the alignment of interface-1 results in alternating positive and negative charges throughout the helical bundle, electrostatically stitching together in-register interfaces while contributing to heterogeneity when they fall out-of-register (Extended Data Fig. 6c). This tightly aligned electrostatic striation results in a large buried-surface area throughout the sOPA1 dimer in the GDP-AlF_x bound state. For the sOPA1 apo state, the total buried surface area in the dimer is considerably less (1059 $Å^2$), due to a looser interface-1 between stalk domains, and thus has less in-register charge within the interface, with almost half the buried surface area (458 $Å^2$) and an overall wider stalk dimer (48 Å) compared to the GDP-AlF_x state (Extended Data Fig. 2d and Supplementary Table 1). There is very little change in the buried surface area between the

paddle and stalk (interface-2) however, the interface between Pα5 in the paddles (interface-3) is significantly smaller in the apo state (10-14 Å^2), again illustrating a conformational change to tighter packing when nucleotide is bound (Extended Data Fig. 2d,e and Supplementary Table 1). The interfaces between the rungs of the helix, in particular interface-7 between the paddles and interface-8 between the N-terminal domains, also appear to have significant electrostatic contributions (Extended Data Fig. 6e,f). The tetramer Interface-4, in contrast, may be more driven by hydrophobic burial within the interface (Extended Data Fig. 6j).

The novel interfaces and membrane binding surfaces of the sOPA1 structures allow us to predict the molecular basis of how 85 mutants identified in DOA patients lead to disease (Extended Data Fig. 7 and Extended Table 1 and Supplementary Table 1). DOA mutations are present throughout all domains of OPA1 and are mapped onto the sOPA1 monomer structure in Fig. 1c and listed in Extended Data Table 1[14,16,17]. Of the 238 sites with point mutations in OPA1, 37 have multiple substitutions, resulting in 284-point mutants expected to disrupt OPA1 function[14,16-18]. As expected, a large number of mutants (121) are localized in the GTPase domain[17] with the rest scattered throughout the structure. In the monomer, 84 mutations are positioned within the hinge regions between domains and may disturb proper protein folding, oligomerization, and the powerstroke. There are 101 DOA mutations that disrupt charged residues, 39 that are proline or glycine helix breakers, and 15 that introduce cysteines. For sOPA1-GDP-AlFx, the majority of sites (187, 87%) are surface exposed and have the potential to disrupt interfaces or membrane binding in an OPA1 assembly, with 85 being within the membrane binding sites or assembly interfaces identified in this paper. Of the 85 mutants, 64 are located in the protein:protein interfaces involved in helical assembly, indicating a strong pathogenicity to mutations within the dimeric sOPA1 interfaces, 17 are membrane facing within the paddle and could disrupt lipid binding, and 21 mutants are likely involved in GTP hydrolysis. Intriguingly, an additional 24 DOA point mutations are located just 1-2 amino acids away from our tightly defined interfaces. Locations of these mutants are summarized in Extended Data Fig. 7 and Extended Data Table 1 and Supplementary Table 1. These observations illustrate the importance of membrane binding and helical assembly in OPA1 pathogenicity.

To determine the cellular impact of disrupting the sOPA1 dimeric and higher-order interfaces we transfected OPA1-GFP mutants into HeLa cells and characterized the resulting mitochondrial morphology (Fig. 4 and Extended Data Fig. 8). In total, we assayed 12 interfacial and membrane binding mutants, spanning six interfaces and two membrane binding helices (Pα2 and Pα6), 11 of which contained atrophy mutants. Compared to WT, which as expected displayed a mix of intermediate and filamentous mitochondria, all tested OPA1 mutants displayed strongly fragmented phenotypes (Fig. 4, and Extended Data Fig. 8). The presence of strongly fragmented mitochondria for all tested interfaces underlies the apparent relevance of the OPA1 higher-order assemblies *in vivo*, and also supports the assertion that many of the observed atrophy mutations stem from the disruption of these oligomeric interfaces.

Given these results, we propose a model where like its counterpart DRP1 in the outer mitochondrial membrane, OPA1 exists in many fluid assembly states during the IMM fusion process (Fig. 5)[20,21,36]. Previous work has shown that OPA1 interacts with the IMM through transmembrane tethering and interaction with the cardiolipin specific paddle domain[1,24,37]. The transmembrane domain of the long form of OPA1 may provide the initial localization of OPA1 to the fusion site, acting as a nucleation site for soluble sOPA1 assembly[2,13]. Once localized to the membrane surface, sOPA1 dimers would assemble through interfaces 1-3 in the stalks and paddles. This is followed by dimer:dimer (interface-4 and -9) and inter-rung (interface-7 and -8)

interactions to generate a helical assembly, inducing bilayer curvature. At this stage, the loosely connected assemblies are stabilized by electrostatic contacts and shallow membrane insertion. Upon GDP-AlF_x binding, the GTPase dimer (interface-5) and a new GTPase-stalk connection (interface-6) form, which tighten the other interfaces in the stalks and paddles, increasing their surface area and forcing deeper insertion of the hydrophobic paddle helices into the bilayer[38,39]. This insertion would drive mechanical destabilization of the bilayer and change the ordering of the cardiolipin. Concurrently, the helical assembly provides a scaffold around the underlying highly curved membrane originating from each mitochondrion until the bilayers are close enough for fusion. What occurs after nucleotide release and further rounds of GTP hydrolysis remains elusive. It is likely OPA1 undergoes a powerstroke like other DSPs, which may be involved in the disassembly of the organized helix and allow for lipid mixing necessary for membrane fusion.

References

1 Chan, D. C. Mitochondrial Fusion and Fission in Mammals. *Annual Review of Cell and Developmental Biology* **22**, 79-99, doi:10.1146/annurev.cellbio.22.010305.104638 (2006).

2 Gao, S. & Hu, J. Mitochondrial Fusion: The Machineries In and Out. *Trends Cell Biol* **31**, 62-74, doi:10.1016/j.tcb.2020.09.008 (2021).

3 Horvath, S. E. & Daum, G. Lipids of mitochondria. *Prog Lipid Res* **52**, 590-614, doi:10.1016/j.plipres.2013.07.002 (2013).

4 Mishra, P. & Chan, D. C. Mitochondrial dynamics and inheritance during cell division, development and disease. *Nat Rev Mol Cell Biol* **15**, 634-646, doi:10.1038/nrm3877 (2014).

5 Francy, C. A., Clinton, R. W., Fröhlich, C., Murphy, C. & Mears, J. A. Cryo-EM Studies of Drp1 Reveal Cardiolipin Interactions that Activate the Helical Oligomer. *Sci Rep* **7**, 10744, doi:10.1038/s41598-017-11008-3 (2017).

6 Macdonald, P. J. *et al.* A dimeric equilibrium intermediate nucleates Drp1 reassembly on mitochondrial membranes for fission. *Mol Biol Cell* **25**, 1905-1915, doi:10.1091/mbc.E14-02-0728 (2014).

7 Stepanyants, N. *et al.* Cardiolipin's propensity for phase transition and its reorganization by dynamin-related protein 1 form a basis for mitochondrial membrane fission. *Mol Biol Cell* **26**, 3104-3116, doi:10.1091/mbc.E15-06-0330 (2015).

8 Fröhlich, C. *et al.* Structural insights into oligomerization and mitochondrial remodelling of dynamin 1-like protein. *Embo j* **32**, 1280-1292, doi:10.1038/emboj.2013.74 (2013).

9 Song, Z., Ghochani, M., McCaffery, J. M., Frey, T. G. & Chan, D. C. Mitofusins and OPA1 mediate sequential steps in mitochondrial membrane fusion. *Mol Biol Cell* **20**, 3525-3532, doi:10.1091/mbc.e09-03-0252 (2009).

10 Zhang, Y. & Chan, D. C. New insights into mitochondrial fusion. *FEBS Lett* **581**, 2168-2173, doi:10.1016/j.febslet.2007.01.095 (2007).

11 Del Dotto, V. & Carelli, V. Dominant Optic Atrophy (DOA): Modeling the Kaleidoscopic Roles of OPA1 in Mitochondrial Homeostasis. *Front Neurol* **12**, 681326, doi:10.3389/fneur.2021.681326 (2021).

12 Del Dotto, V., Fogazza, M., Carelli, V., Rugolo, M. & Zanna, C. Eight human OPA1 isoforms, long and short: What are they for? *Biochim Biophys Acta Bioenerg* **1859**, 263-269, doi:10.1016/j.bbabio.2018.01.005 (2018).

13 Lee, H. & Yoon, Y. Mitochondrial Membrane Dynamics—Functional Positioning of OPA1. *Antioxidants* **7**, 186 (2018).

14 Le Roux, B. *et al.* OPA1: 516 unique variants and 831 patients registered in an updated centralized Variome database. *Orphanet J Rare Dis* **14**, 214, doi:10.1186/s13023-019-1187-1 (2019).

15 Landes, T. *et al.* OPA1 (dys)functions. *Seminars in Cell & Developmental Biology* **21**, 593-598, doi:https://doi.org/10.1016/j.semcdb.2009.12.012 (2010).

16 Weisschuh, N. *et al.* Mutation spectrum of the OPA1 gene in a large cohort of patients with suspected dominant optic atrophy: Identification and classification of 48 novel variants. *PLoS One* **16**, e0253987, doi:10.1371/journal.pone.0253987 (2021).

17 Li, D., Wang, J., Jin, Z. & Zhang, Z. Structural and evolutionary characteristics of dynamin-related GTPase OPA1. *PeerJ* **7**, e7285, doi:10.7717/peerj.7285 (2019).

18 Ban, T., Heymann, J. A., Song, Z., Hinshaw, J. E. & Chan, D. C. OPA1 disease alleles causing dominant optic atrophy have defects in cardiolipin-stimulated GTP hydrolysis and membrane tubulation. *Hum Mol Genet* **19**, 2113-2122, doi:10.1093/hmg/ddq088 (2010).

19 Yapa, N. M. B., Lisnyak, V., Reljic, B. & Ryan, M. T. Mitochondrial dynamics in health and disease. *FEBS Lett* **595**, 1184-1204, doi:10.1002/1873-3468.14077 (2021).

20 Faelber, K. *et al.* Structure and assembly of the mitochondrial membrane remodelling GTPase Mgm1. *Nature* **571**, 429-433, doi:10.1038/s41586-019-1372-3 (2019).

21 Zhang, D. *et al.* Cryo-EM structures of S-OPA1 reveal its interactions with membrane and changes upon nucleotide binding. *Elife* **9**, doi:10.7554/eLife.50294 (2020).

22 Wang, R. *et al.* Identification of new OPA1 cleavage site reveals that short isoforms regulate mitochondrial fusion. *Mol Biol Cell* **32**, 157-168, doi:10.1091/mbc.E20-09-0605 (2021).

23 Anand, R. *et al.* The i-AAA protease YME1L and OMA1 cleave OPA1 to balance mitochondrial fusion and fission. *J Cell Biol* **204**, 919-929, doi:10.1083/jcb.201308006 (2014).

24 Ge, Y. *et al.* Two forms of Opa1 cooperate to complete fusion of the mitochondrial inner-membrane. *eLife* **9**, e50973, doi:10.7554/eLife.50973 (2020).

25 Ingerman, E. *et al.* Dnm1 forms spirals that are structurally tailored to fit mitochondria. *J Cell Biol* **170**, 1021-1027, doi:10.1083/jcb.200506078 (2005).

26 Kong, L. *et al.* Cryo-EM of the dynamin polymer assembled on lipid membrane. *Nature* **560**, 258-262, doi:10.1038/s41586-018-0378-6 (2018).

27 Yan, L. *et al.* Structural analysis of a trimeric assembly of the mitochondrial dynamin-like GTPase Mgm1. *Proceedings of the National Academy of Sciences* **117**, 4061-4070, doi:doi:10.1073/pnas.1919116117 (2020).

28 Faelber, K. *et al.* Crystal structure of nucleotide-free dynamin. *Nature* **477**, 556-560, doi:10.1038/nature10369 (2011).

29 Yu, C. *et al.* Structural insights into G domain dimerization and pathogenic mutation of OPA1. *Journal of Cell Biology* **219**, doi:10.1083/jcb.201907098 (2020).

30 Punjani, A., Zhang, H. & Fleet, D. J. Non-uniform refinement: adaptive regularization improves single-particle cryo-EM reconstruction. *Nature Methods* **17**, 1214-1221, doi:10.1038/s41592-020-00990-8 (2020).

31 Zhong, E. D., Bepler, T., Berger, B. & Davis, J. H. CryoDRGN: reconstruction of heterogeneous cryo-EM structures using neural networks. *Nature Methods* **18**, 176-185, doi:10.1038/s41592-020-01049-4 (2021).

32 Jimah, J. R. & Hinshaw, J. E. Structural Insights into the Mechanism of Dynamin Superfamily Proteins. *Trends in Cell Biology* **29**, 257-273, doi:https://doi.org/10.1016/j.tcb.2018.11.003 (2019).

33 Krissinel, E. & Henrick, K. Inference of macromolecular assemblies from crystalline state. *J Mol Biol* **372**, 774-797, doi:10.1016/j.jmb.2007.05.022 (2007).

34 Chappie, J. S. *et al.* A pseudoatomic model of the dynamin polymer identifies a hydrolysis-dependent powerstroke. *Cell* **147**, 209-222, doi:10.1016/j.cell.2011.09.003 (2011).

35 Chappie, J. S., Acharya, S., Leonard, M., Schmid, S. L. & Dyda, F. G domain dimerization controls dynamin's assembly-stimulated GTPase activity. *Nature* **465**, 435-440, doi:10.1038/nature09032 (2010).

36 Mears, J. A. *et al.* Conformational changes in Dnm1 support a contractile mechanism for mitochondrial fission. *Nat Struct Mol Biol* **18**, 20-26, doi:10.1038/nsmb.1949 (2011).
37 Ge, Y., Boopathy, S., Nguyen, T. H., Lugo, C. M. & Chao, L. H. Absence of Cardiolipin From the Outer Leaflet of a Mitochondrial Inner Membrane Mimic Restricts Opa1-Mediated Fusion. *Frontiers in Molecular Biosciences* **8**, doi:10.3389/fmolb.2021.769135 (2021).
38 Ban, T. *et al.* Molecular basis of selective mitochondrial fusion by heterotypic action between OPA1 and cardiolipin. *Nat Cell Biol* **19**, 856-863, doi:10.1038/ncb3560 (2017).
39 Osman, C., Voelker, D. R. & Langer, T. Making heads or tails of phospholipids in mitochondria. *Journal of Cell Biology* **192**, 7-16, doi:10.1083/jcb.201006159 (2011).

Main Text Figures

Figure 1

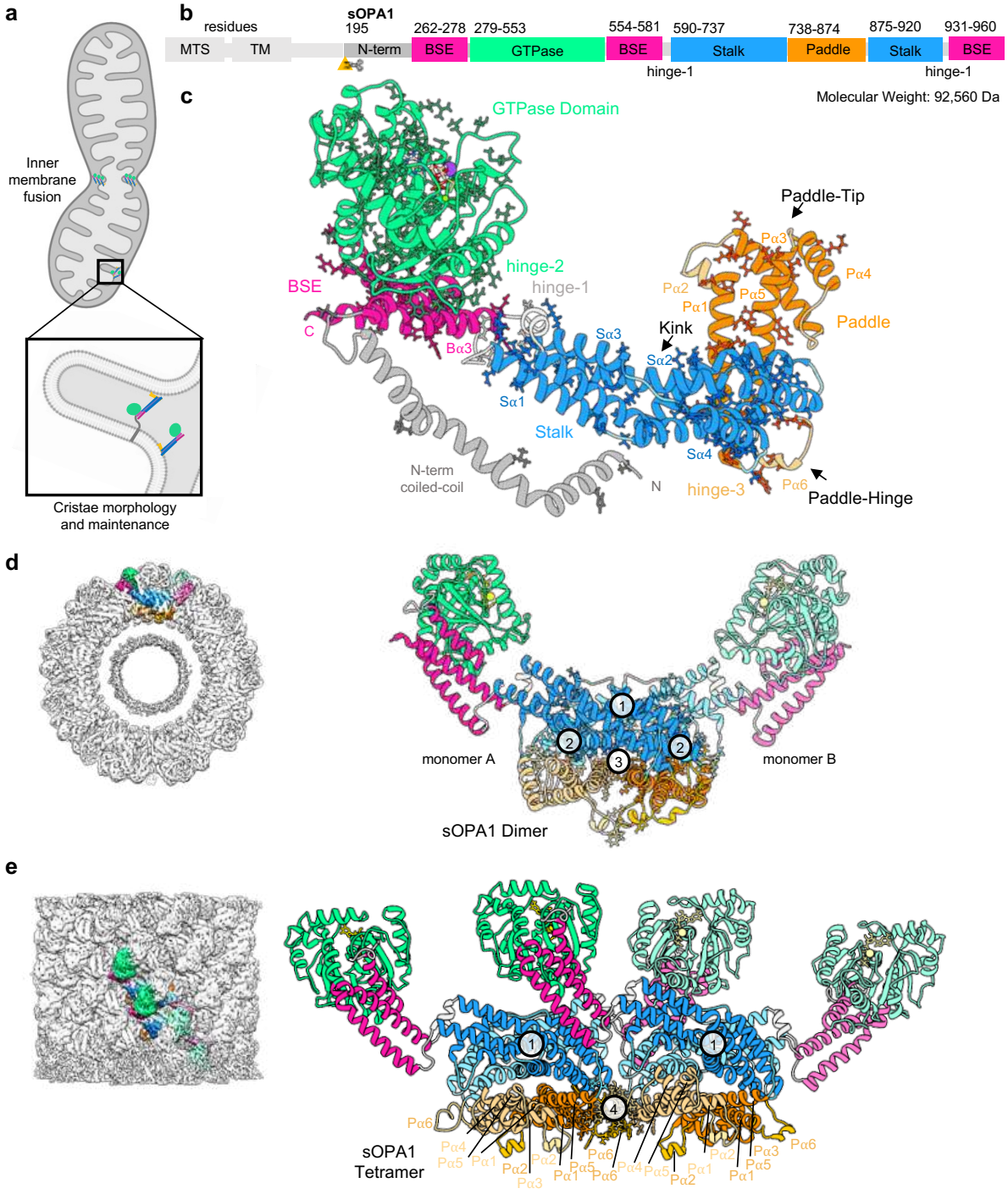

Figure 1, Oligomeric interfaces within the cryoEM helical structure of OPA1, the mitochondrial inner membrane fusion and cristae remodeling protein. **a**, Cartoon of two fusing mitochondria. OPA1 is depicted in its dual inner mitochondrial membrane (IMM) fusion (top) and cristae morphological regulation roles (bottom inset). OPA1 is colored by domain (GTPase:green, BSE:pink, stalk:blue, paddles:orange, hinge-1:light gray, N-term:dark gray) in both long and short forms. **b**, Sequence diagram colored by domain with residues labeled above. The OPA1 isoform-1 S1 cleavage site is shown with a yellow arrow at residue 195. **c,** Model of sOPA1-GDP-AlF_x. Kinks and turns in the stalk are colored light blue and membrane inserting regions are colored a lighter orange in the paddle. Point mutations resulting in Dominant Optic Atrophy are colored by domain (as in b) and shown as sticks. Alpha-helices are labeled according to the sequence diagram in Supplementary Fig. 1. sOPA1 assembles into a biological dimer, with 3 distinct interfaces (circled numbers). Interface-1: between the stalks of the monomers. Interface-2: between the stalk and paddle of the opposing monomers. Interface-3: between the paddles of the dimer (denoted monomer A and B). Monomer A is colored as in **a** and monomer B is shown in lighter hues. Left shows a dimer within the helical map for orientation. **e**, sOPA1 tetramer (dimer-of-dimers) forms through a 4^{th} interface between the paddle-hinges of monomer A from dimer-1 and monomer B from dimer-2. Left shows a tetramer within the helical map. Paddle alpha-helices are labeled as in Supplementary Fig. 1.

Figure 2

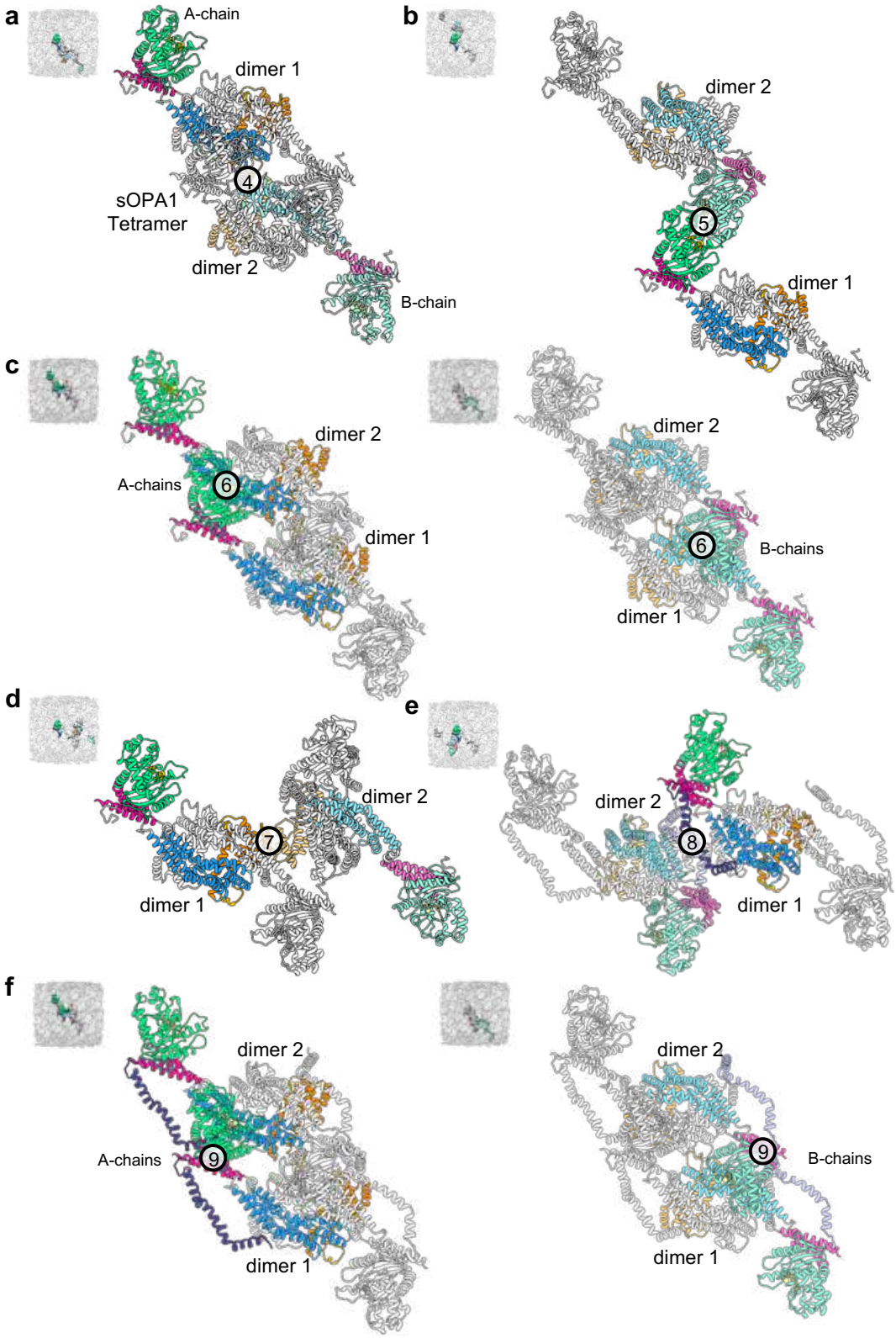
a
A-chain
dimer 1
4
sOPA1
Tetramer
dimer 2
B-chain
b
dimer 2
5
dimer 1
c
dimer 2
A-chains
6
dimer 1
dimer 2
6
B-chains
dimer 1
d
dimer 2
7
dimer 1
e
dimer 2
8
dimer 1
f
dimer 2
A-chains
9
dimer 1
dimer 2
9
B-chains
dimer 1

Figure 2: The interfaces involved in sOPA1 helical assembly. (a-g) Defining the interfaces between sOPA1 dimers. In each case, the sOPA1 monomers involved in the interface are colored by domain (see Fig. 1) with chain A and B a darker and lighter hue respectively**.** sOPA1s chains not involved in the interfaces are colored gray. Left, insets show the sOPA1 units in the context of the full helical map. **a,** dimers of sOPA1 assemble into a tetramer through interface-4. **b,** In the presence of GDP-AlF_x, two dimers beyond the tetramer in the biological rung of the helix form a GTPase domain dimer (interface-5) between dimer-1 A-chain and dimer-2 B-chain**. c,** In the presence of GDP-AlF_x, the two dimers within the tetramer are further connected between the GTPase and stalk domains (interface-6) by dimer-1 A-chain and dimer-2 A-chain (left) or dimer-1 B-chain and dimer-2 B-chain (right)**. d,** Interface-7 connects the rungs of the helix through the paddle domains. **e,** A second interface between the adjacent rungs (interface-8), involves an N-terminal a coiled-coiled domain between dimer-1 A-chain and dimer-2 B-chain. **f,** A third interface within the tetramer exists between the N-terminal helix and the BSE (interface-9) from dimer-1 A-chain and dimer-2 A-chain (left) or dimer-1 B-chain and dimer-2 B-chain (right)**.** Interfaces were determined using PDBePISA and displayed in Chimera[33,40].
coiled-coils of dimer-1 A-chain and dimer-2 B-chain. **f,** The two dimers within the tetramer in the biological rung of the helix form a N-terminus:BSE dimer (interface-9) between dimer-1 A-chain and dimer-2 A-chain (left) or dimer-1 B-chain and dimer-2 B-chain (right)**.** Interfaces were determined using PDBePISA[33].

Figure 3

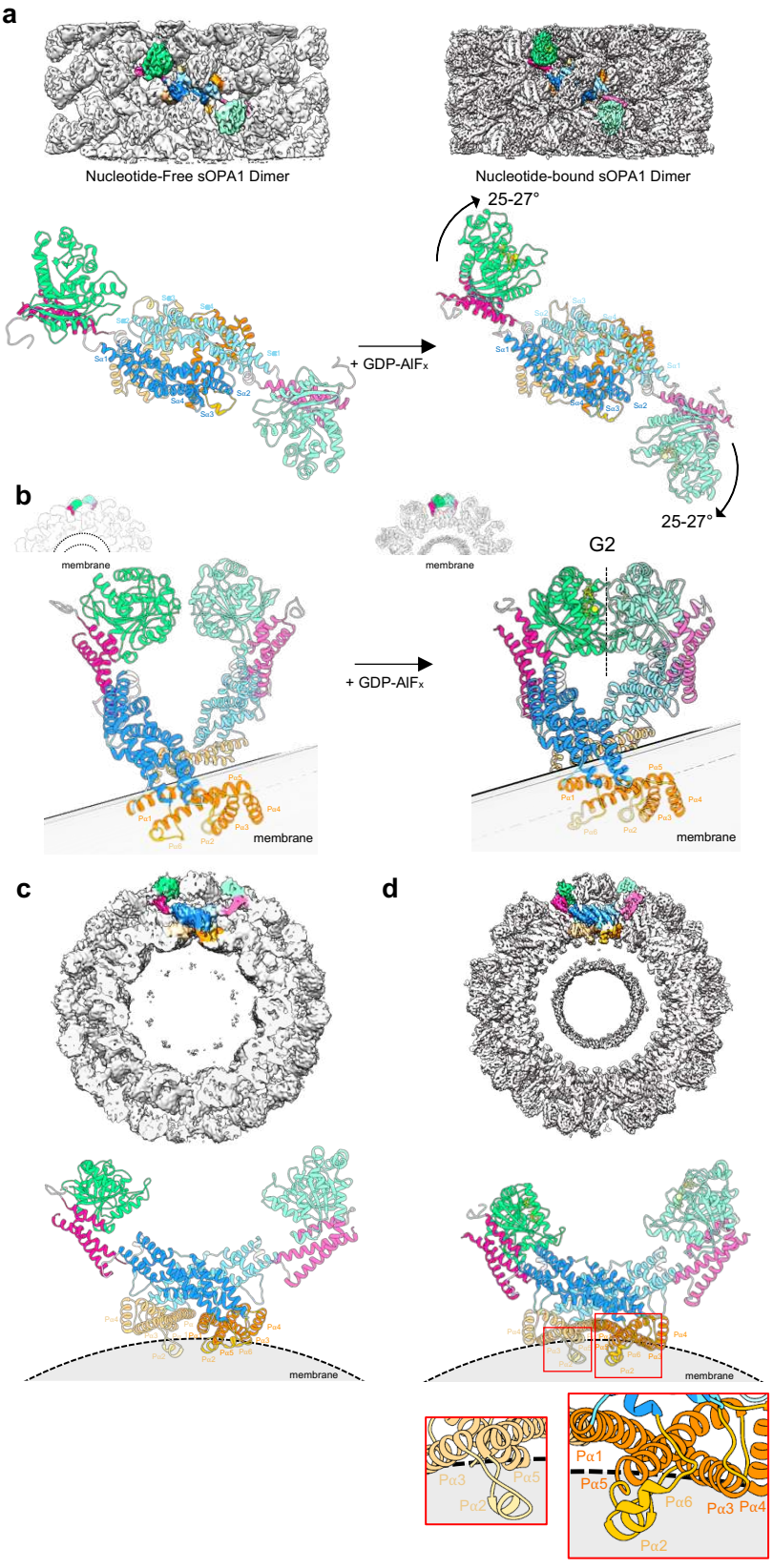
a
Nucleotide-Free sOPA1 Dimer
Nucleotide-bound sOPA1 Dimer
25-27°
+ GDP-AlFx
25-27°
b
membrane
membrane
G2
+ GDP-AlFx
membrane
membrane
c
d
membrane
membrane
Pα1
Pα5
Pα6
Pα3 Pα4
Pα2
Pα3
Pα5
Pα2

Figure 3: A comparison of sOPA1 dimers and assembly in the apo and GDP-AlF$_x$ bound states. a, Side view of sOPA1 apo (left) and GDP-AlFx (right) helical structures with a dimer of sOPA1 colored by domain and models below highlighting the transition from the apo to the GDP-AlF$_x$ states - a shift to more compact stalk and paddle interfaces and a 25-27° swing in the GTPase domains. Helices are labeled as in the sequence alignment in Supplementary Fig. 1**. b,** The transition from apo (left) to GDP-AlF$_x$ (right) results in a GTPase dimer through interface-5. Clipped maps are shown in the top left corners and the membrane positioning is highlighted in gray. **c,** Top view of the sOPA1 apo helical structure with a dimer of sOPA1 colored by domain. Minimal membrane insertion of helices Pa2 and Pa6 shown below. **d,** Top view of sOPA1 GDP GDP-AlF$_x$ helical structure with the model below revealing a deeper membrane insertion a-helices Pa2 and Pa6 and a closer membrane contact with Pa1 and Pa5 (insets)**.**

Figure 4

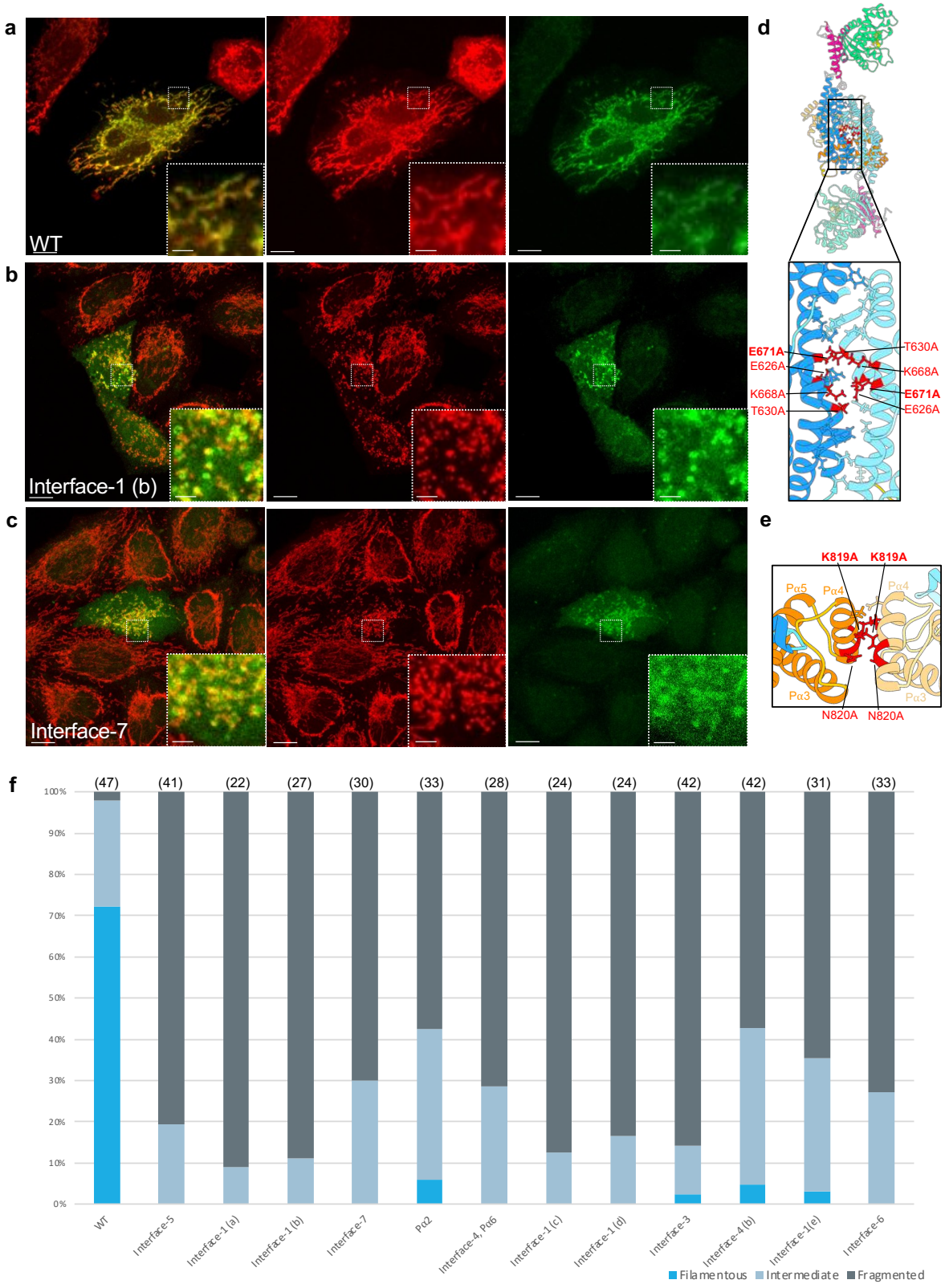
a
WT
b
Interface-1 (b)
c
Interface-7
d
E671A
E626A
K668A
T630A
T630A
K668A
E671A
E626A
e
K819A
K819A
Pα5
Pα4
Pα4
Pα3
Pα3
N820A
N820A
f
(47)
(41)
(22)
(27)
(30)
(33)
(28)
(24)
(24)
(42)
(42)
(31)
(33)
100%
90%
80%
70%
60%
50%
40%
30%
20%
10%
0%
WT
Interface-5
Interface-1 (a)
Interface-1 (b)
Interface-7
Pα2
Interface-4, Pα6
Interface-1 (c)
Interface-1 (d)
Interface-3
Interface-4 (b)
Interface-1(e)
Interface-6
Filamentous
Intermediate
Fragmented

Figure 4: Examining the functional impact of interfaces between OPA1 in assembly and membrane binding. a-c, Images of HeLa cells transfected with WT or mutant OPA1-GFP. Colocalization of OPA1-GFP (green) and mitochondria stained with MitoTracker (red) (left) followed by MitoTracker alone (middle) and OPA1-GFP alone (right). **a**, WT Opa1 showing filamentous and intermediate length mitochondria. **b,** Images of HeLa cells transfected with OPA1-GFP interface-1 mutant (E626A, T630A, K668A, E671A) OPA1-GFP show fragmentation of the mitochondrial network. **c,** Images of HeLa cells transfected with OPA1-GFP interface-7 mutant (K819A, N820A) also show fragmentation of the mitochondrial network. **d,** Model of the OPA1 dimer colored by chain with H-bonds within interface-1 shown and residues mutated in the interface-1(b) mutant colored red. **e,** Model of interface-6 where H-bonding residues are shown in sticks and residues mutated colored red and labeled. **f,** Table summarizing mitochondrial network fragmentation for each mutated interface. Mitochondrial networks were measured and categorized as filamentous (blue), intermediate (light blue), or fragmented (gray) and plotted as a percentage of total cells. Cell counts appear above each bar. The alanine mutations introduced into the OPA1-GFP sequence were: E444A (Interface-5), R627A:K663A:R683A Interface-1(a), E626A:T630A:K668A:E671A (Interface-1 (b), Q659A (Interface-1(c), E679A (Interface-1(d), H631A (Interface-1(e), K819A:N820A(Interface-7), W771A:K772A:K773A:R774A:W775A:L776A:Y777A:W778A:K779A:N780A:R781A (Pα2), F860A:Y861A:Y862A:Y863A:Q864A:R865A:H866A:F867A (Pα6, and Interface-4), I735A (Interface-4(b), K614A:H615A:D835A (Interface-2), and D716A (Interface-6). Sites with DOA mutations are bolded in **d** and **e**. Detailed images for each interface mutant can be seen in Extended Data Figure 8.

Figure 5

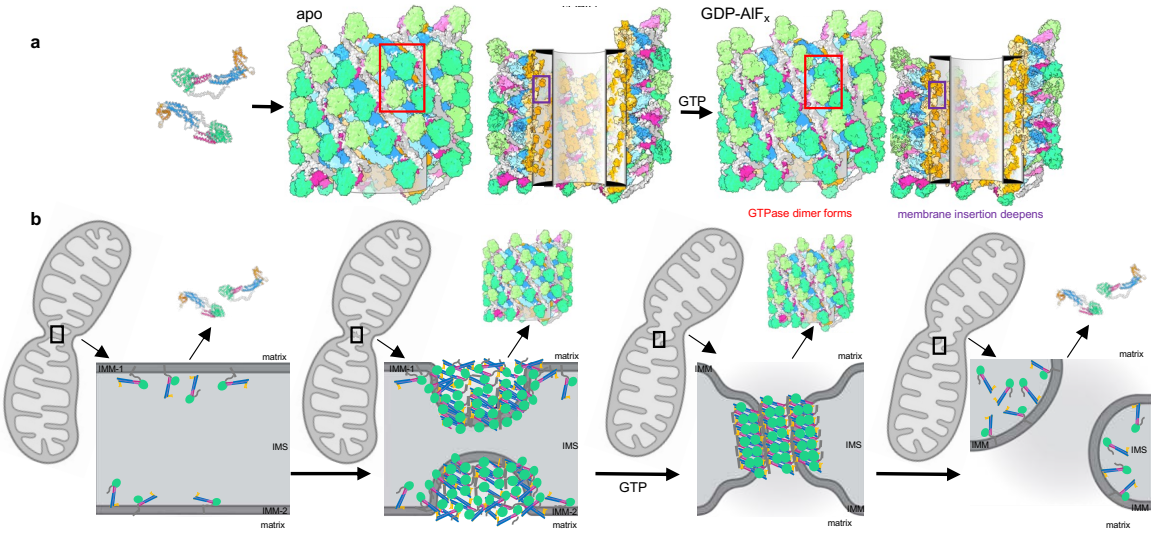

Figure 5: A model of inner membrane fusion by sOPA1. a, sOPA1 monomers assemble into loose helical assembly in the apo state that transitions to a more compact structure upon GTP addition. Both surface and clipped views of the apo and GDP-AlFx helical assemblies of sOPA1 are shown highlighting membrane insertion (purple box) that deepens in the nucleotide state. Furthermore, the GTPase domains dimerize (interface-5) (red box) in the GDP-AlFx state. See Extended Data Movie 1 for a detailed morph between the two states. **b,** A cartoon of OPA1 assembly in the mitochondria during mitochondrial fusion. Panel 1, OMM fusion joins the IMS of two mitochondria and brings two IMM in proximity. OPA1 proteins from the two mitochondria exist in dynamic oligomers in the IMS proximal to their respective IMM. The sOPA1 oligomers contact the IMM through their paddle domains and interact with membrane-anchored, full-length OPA1. Panel 2, upon the proper mitochondrial stimulus, apo OPA1 enters a primed state where it assembles into two flexible helices of varying diameter on the IMM bilayers, causing IMM deformation. Panel 3, nucleotide-binding orders and tightens the helical assemblies, deepening insertion into the bilayer and promoting fusion. Panel 4, fusion occurs before or after OPA1 helices disassemble. OMM and IMM are colored dark gray, IMS is medium gray and the matrix is light gray. Above insets (arrows) showsOPA1 monomers, and apo and GDP-AlFx helical structures (see Extended Data Movie 1). Mitochondrial cartoons were created with BioRender.com.

Extended Data Figures and Tables

Extended Data Figure 1

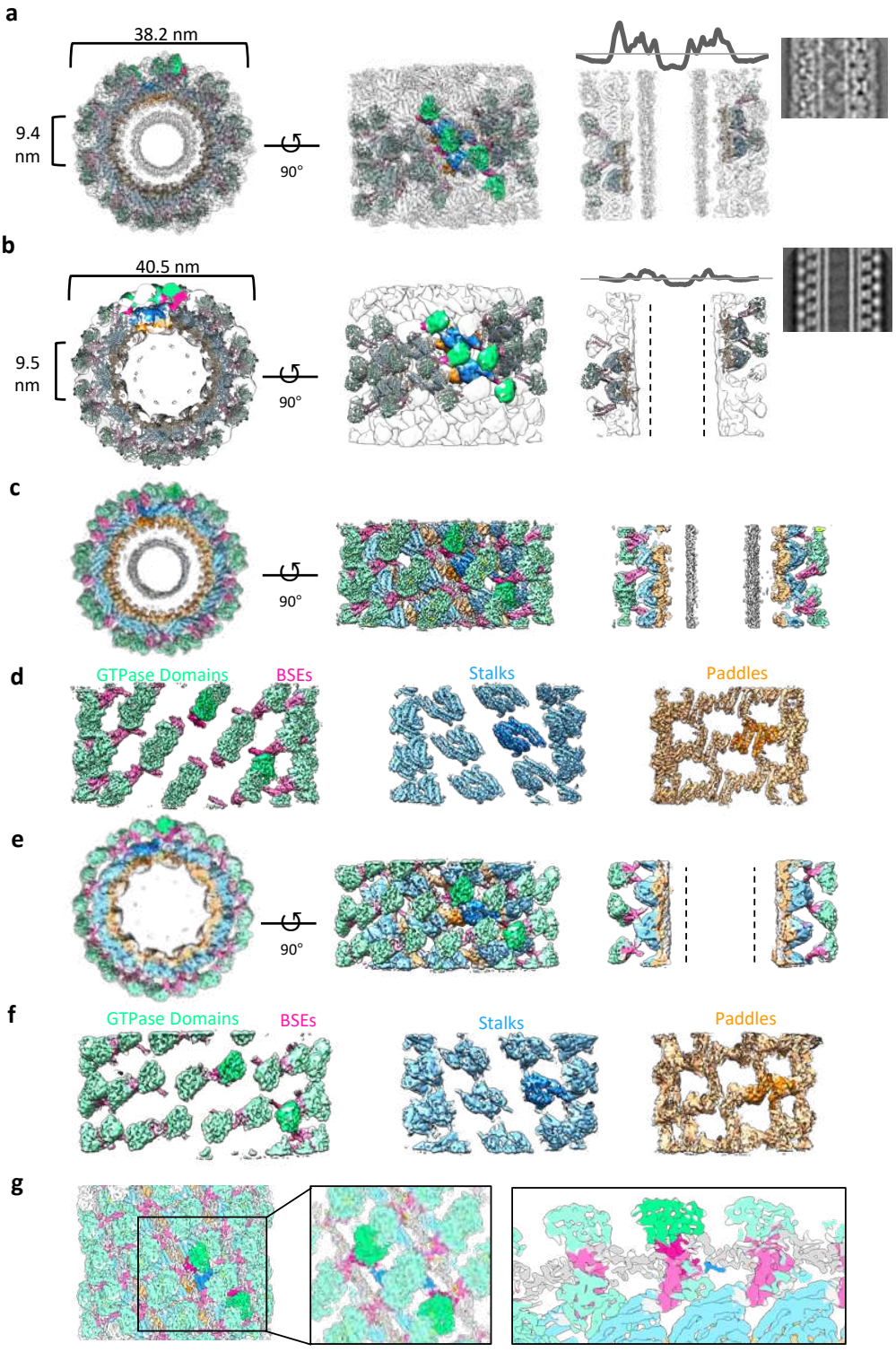

Extended Data Figure 1: Helical Assemblies of sOPA1 coating cardiolipin containing membranes with and without GDP-AlF$_x$. a, Left, top view of sOPA1 with GDP-AlF$_x$ bound, with 38.2 nm helical diameter and a 9.4 nm diameter membrane. Top-center, A 90° rotation of the left panel. The 10 modeled tetramers which define a single helical turn are colored by domain (GTPase:green, BSE:pink, stalks:blue, paddles:orange). Right, a clipped slice of the helix is shown in comparison to a corresponding 2D classification generated in RELION (right-corner). A radial profile plot is shown above the sliced helix. **b,** Left, top view of sOPA1 preceding GDP-AlF$_x$ addition, with 40.5 nm helical diameter and a 9.5 nm diameter membrane. Top-center, A 90° rotation of the left panel. The 10 modeled tetramers which define a single turn are colored as in **a**. Right, a central slice of the helix is shown in comparison to a corresponding 2D classification generated in RELION (right-corner). A radial profile plot is shown above the sliced helix. **c,** A Z-clipped refinement focusing on the central ~30% of the GDP-AlF$_x$ bound helix is colored by domain, shown as a top view at left, then rotated 90-degrees and centrally sliced at right with a single sOPA1 dimer highlighted in darker hues. **d,** Domains are colored and zoned moving from the outer diameter of the helix toward the membrane bilayer. Left, the GTPase domains and BSE regions are colored green and pink, respectively. Middle, the stalks are shown in blue. Right, the paddles are colored orange. **e,** same as **c** for the apo helix. **f,** same as in **d** for the apo helix. **g,** A GDP-AlF$_x$ bound helical map with density colored by domain, refined in cryoSPARC without dynamic masking. A zoomed inset shows the N-term in gray.

Extended Data Table 1

position (res no.)	WT seq (aa)	disease mutant (aa)	position (res no.)	WT seq (aa)	disease mutant (aa)	position (res no.)	WT seq (aa)	disease mutant (aa)	position (res no.)	WT seq (aa)	disease mutant (aa)
8	A	S	332[d]	S	E*	501	V	D	728	N	K
15	Q	K	337	H	D	502[b,d]	V	G	730	L	F
24	I	V	339	A	T, D	503[b]	T	K	735[a]	I	M
29	P	H*	340	L	P, Y*	505[a,b]	K	N	736[a]	S	L*
61	Q	R	342	K	E	515	I	K*	740	Q	L*
80	Y	H, C	343	D	A	517	E	I*	745[a,c,d]	I	M
82	Y	C	346	R	Q, G*	518	Y	N*	746[a,c]	Y	L*
85	R	H	357	A	T, L*	521	E	D*	747[a]	F	L*
95	T	M	358	A	F*	524	Q	R, L, S*	755[a]	R	C
101	R	Q*	366	R	Q	534	L	R	756[c]	L	P
102	Y	C	371	V	G	541	T	A	759	T	M
115	A	V	376[a]	T	A	545	S	R	765[a]	N	K*
119	F	S	377	V	I	547	A	E	768	G	S, D
125	M	T	380	E	D	548[d]	V	I, F*	770[c]	D	E
127	P	L	381	T	S	549	S	I, F*	781[c]	R	W
132	Y	I*	382	I	M	550	D	N	783[c]	Q	R, P*
150	E	V*	384	L	F	551	C	Y	785[c]	Q	R
158	S	N	385	N	C, R*	553	W	G*	786[c]	C	F*
160	E	Q	391	L	R	554	K	N*	789[c]	N	S, M*
167	P	L	394[d]	M	V	556[d]	V	E, S*, Q*	819[a]	K	R*
187	S	A*	395	V	G	557[a]	R	P, Y*	823[a,c]	S	Y
189	E	G*	396	L	P, R	565[a]	D	I*	831[a]	S	N
191	T	M	399[d]	L	Y*	571	R	H	832[a]	L	F
192	A	V	400	P	A, L, S	574	L	P	833[d]	I	L*
196	T	N*	401[b,d]	G	R, D	575	E	K	841[a]	Y	C
205[a]	H	L*	402[a]	V	M	582	Y	C	843[c]	R	S
211	D	K*	404[a]	N	K*	585	L	R*	846	L	F*
212[a]	K	R*	405[a]	T	I*	590	R	Q, W	852[c]	H	T*
213[a]	E	R*	409[a]	G	D	592	E	Q*	856[d]	C	N*
214[d]	K	N*	410[a]	M	H*	593	L	P	863[a,c]	Y	I*
222	L	P	418	I	F	594	F	K*	864[a,c]	Q	P*
235	R	Q	422	S	R	595	E	G*	872[a,c]	L	W*
252	D	E*	426	M	L	601	I	V	873[a]	E	G*
260	L	F	428	N	H, D	609	S	A*	880	F	A*
265	I	T*	430[a]	N	D	612[a]	T	Q*	881	W	L*
268	Y	C	431	A	S*	617	E	L*	882	R	L, C, G
269	S	F	434[a,b,d]	L	P, R	627[a]	R	E*, S*	885	R	H
270	E	K	435[d]	C	R,Y	631[a]	H	R*	887	L	P
272	L	P, F	443[a]	A	T	646	S	L	894	L	F*
273	D	A	444[a]	E	G	652	T	A	901	T	I, L*
280	A	V*	445[a]	R	L, H	653[d]	V	G	903	V	L, I, G, E*
285	Q	R	446[a]	S	C	654	D	G, V*	907	E	G
290	R	Q, W, L	449[a]	T	R, P	656[a]	K	S*	909	N	C*
292[d]	V	F	450[b]	D	R*	659[a]	Q	T*	910[d]	V	D
296[a]	D	E	452[d]	V	S*	662	D	V*	921	G	C
298[a,b]	S	N, G	457	P	T	663[a]	K	N*	924	K	R*
299[b]	A	P	459	G	E	666[d]	P	L*	928	L	P
300[b]	G	E	462[d]	T	I	671[a]	E	A	929	T	S
302[b]	T	P	465[d]	V	F	672	V	L*	932	R	C, L*
303[b]	S	N	468[a,b]	K	E	673[d]	A	R*	933[d]	V	F
310	Q	R	469[a]	V	I	677[d]	L	Y*	934	Q	P*
311	A	V*	470[a,b]	D	G	683[a]	R	H	939	L	P
313[d]	I	K, E	471[a,b]	L	P	687[a]	E	D*, T*	942	V	S*, E*
317[a,b]	G	D*	482	I	F, G*	699	K	N*	943	R	E*
322[b]	M	R	487	E	K	701	K	R*	949	L	P, R, I, T*
326	P	Q*	488[a,b]	G	R	709[a]	I	G*	950	D	C*
328	K	R	493[d]	M	K	716[a]	D	E	952	F	S*
329[d]	V	L	494	K	I*	717[a]	F	C*	953	I	H*
330	T	S	495	A	V	718	A	E			
331[d]	L	P	499	F	L*	725	I	S*			

Extended Table 1: DOA Mutations currently identified in OPA1[14,16,17]. Sites are colored by domain (dark gray: luminal/MTS, light gray: N-terminal linker before S1 cleavage site, medium gray: N-terminal coiled-coil, magenta: BSE, green: GTPase domain, lightest gray: hinge 1, blue: stalk, orange: paddle). Asterisks note single-point mutations resulting from a frame shift. [a]protein:protein interfaces [b]protein:nucleotide binding [c]membrane binding [d]buried

Extended Data Figure 2

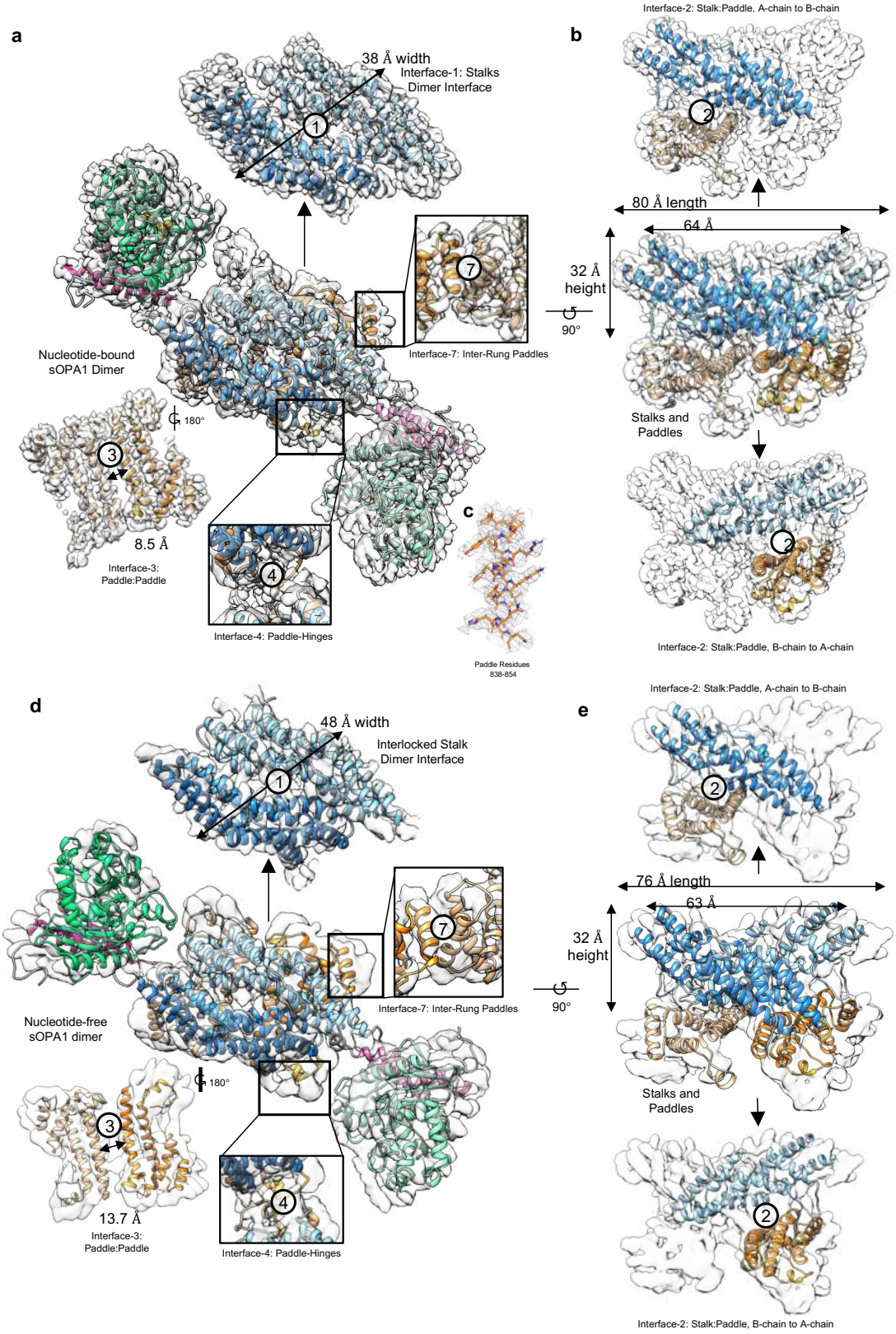

Extended Data Figure 2: A closer examination of the interfaces within the sOPA1 dimer stalks and paddles. a, A side view of a GDP-AlF_x sOPA1 dimer fit into the locally refined map, colored by chain. GTPase domains are colored dark green (chain A) and light green (chain B), BSEs dark pink (chain A) and light pink (chain B), stalks dark blue (chain A) and light blue, (chain B) and paddles dark orange (chain A) and light orange (chain B). Arrows mark the interlocked stalk interface-1 (top) and paddle:paddle interface-3 (bottom). The paddle is rotated 180-degrees and shows the face which contacts the membrane. Interface-4 between the paddle-hinges and interface-7 between the inter-rung paddles are boxed at their locations relative to the sOPA1 dimer. Interfaces are labeled and circled**. b,** Top view of isolated interfaces for the sOPA1 stalk and paddle regions. The full dimeric interface between the stalks and paddles is shown fit into the locally refined density and colored as in A. Interface-2 between the stalk of one sOPA1 monomer and the paddle of the second is shown for the A- to B-chain (top) and the B- to A-chain (bottom). Interfaces are labeled and circled**. c,** A representative fit of the paddle residues 838-854 within Pα5 of the sOPA1 model into the map density**. d,** same as in **a** for the apo dimer. **e,** same as in **b** for the apo dimer.

Extended Data Figure 3

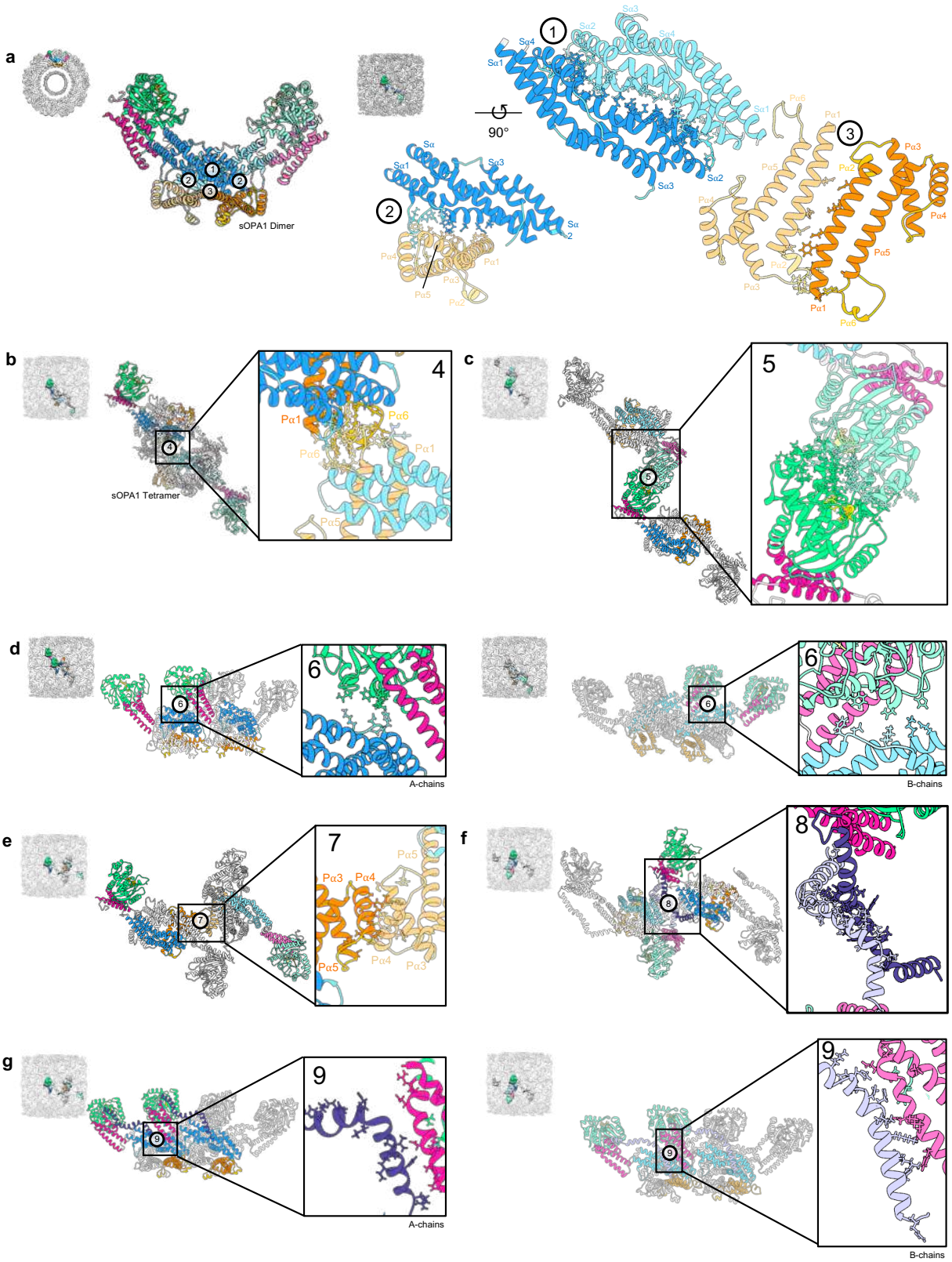

Extended Data Figure 3: The interfaces involved in sOPA1 helical assembly. a, Left, the 3 interfaces that form the sOPA1 dimer. The GTPase domains are colored in dark green (A-chain) and light green (B-chain), BSE region in dark pink (A-chain) and light pink (B-chain), stalks in dark blue (chain A) and light blue (chain B), and paddles in dark orange (chain A) and light orange (chain B**).** Top left, a helical map with a single highlighted dimer. Top middle, a side view of the helical map with a single highlighted dimer. Right, zooms of each interface with buried residues shown as sticks. (**b-g**) Defining the interfaces between sOPA1 dimers. In each case, colors are as in **a**. The chains of each sOPA1 dimer that is not involved in the interface are gray. Left, insets show sOPA1 in the context of the full helical map. Zoomed boxes show the interfaces in more detail. Residues buried in each interface are shown with sticks. **b,** Two dimers of sOPA1 assemble into a tetramer through interface-4. **c,** In the presence of GDP-AlF_x, two dimers form a GTPase domain dimer (interface-5) between dimer-1 A-chain and dimer-2 B-chain**. d,** In the presence of GDP-AlF_x, the two dimers also form a GTPase domain:stalk dimer (interface-6) between dimer-1 A-chain and dimer-2 A-chain (left) or dimer-1 B-chain and dimer-2 B-chain (right)**. e,** Between rungs, two dimers form interface-7 involving paddles of dimer-1 A-chain and dimer-2 B-chain in each dimer**. f,** Another inter-rung interface (interface-8), appears between two dimers through the N-terminal coiled-coils (purple) of dimer-1 A-chain and dimer-2 B-chain. **g,** An N-terminus:BSE dimer interface (interface-9) forms between dimer-1 A-chain and dimer-2 A-chain (left) or dimer-1 B-chain and dimer-2 B-chain (right)**.** Interfaces were determined using PDBePISA[33].

Extended Data Figure 4

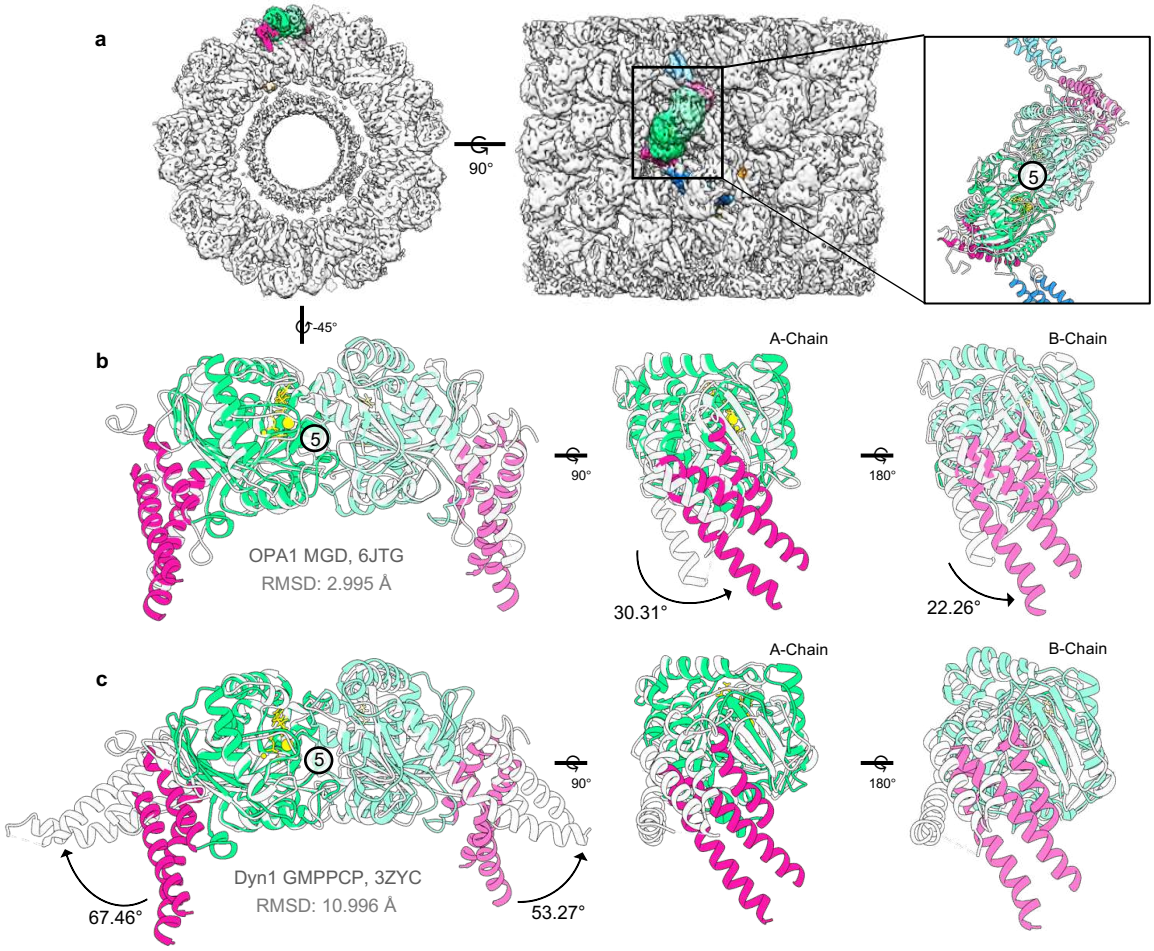

Extended Data Figure 4: Contextualizing the Nucleotide dependent GTPase dimer (Interface-5) in the helical assembly. a, Interface-5, a GTPase dimer of sOPA1 is colored by chain in top (left) and side (right) views. GTPase domains are colored in dark green (chain A) and light green (chain B), BSEs in dark pink (chain A) and light pink (chain B), stalks in dark blue, (chain A) and light blue, (chain B) and paddles in dark orange (chain A) and light orange (chain B). The boxed inset shows both the sOPA1 model and 6JGT dimer (dark gray) fit into the map. Interface-5 is labeled and circled**. b,** Shows the sOPA1 model versus the 6JTG dimer, colored as in A from the top (left) and two side views (center, right) to highlight differences in dimer conformation. The BSE domains of both chains swing to accommodate the angular difference of hinge-1 connecting the stalks, resulting in the A- and B-chains fitting with slight asymmetry compared to the crystal structure. Interface-5 is labeled and circled**. c,** Shows the sOPA1 model versus the Dyn1, 3ZYC dimer with GMPPCP bound, colored as in A from the top (left) and two side views (center, right) to highlight differences in dimer conformation. The orientational difference in the BSE domains is expected from the powerstroke model for DSPs.

Extended Data Figure 5

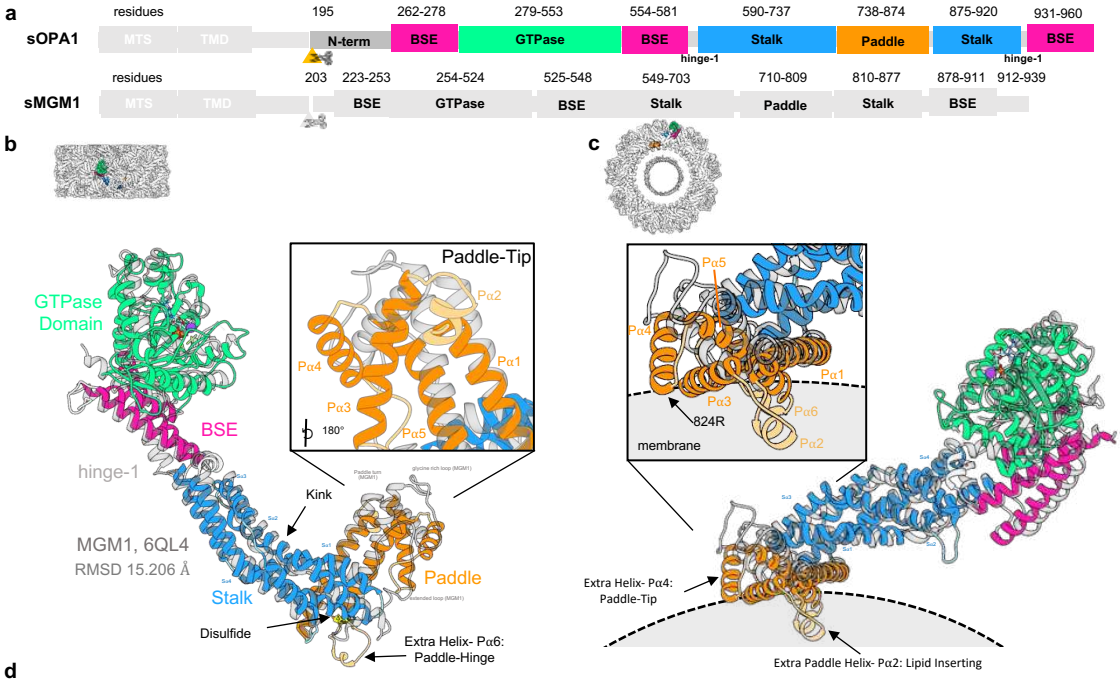

d

OPA1			MGM1		
secondary structure	sequence (AA)	# charged or aromatic AA	secondary structure	sequence (AA)	# charged or aromatic AA
Pα1	738-KQQWDAAIYFMEEALQARLKDTENAIENMV-767	6	Pα1	712-QPNEWAQGREHVVGVLQAELEQCQAAMKALE-742	4
Pα2	768-GPDWKKRWLYWKNRT-782	9	paddle turn	743-NSVGG-747	0
Pα3	783-QEQCVHNETKNELEKMLK-800	4	Pα3	748-RKKLKEVMSFVDKARK-763	8
Pα4	801-CNEEHPAYLASDEITTVRKNLESRGVEVDP-830	5	glycine rich loop	764-GEIIVEGDHPSGAGGFS-780	2
Pα5	831-SLIKDTWHQVYRRHFLKTALNHCNLCRR-858	12	Pα5	781-AALLARGREAVFLRDRADILSLRIQAAKSRQ-808	8
Pα6	859-GFYYYQRHFVDSELE-873	7	Pα6	813-KTLTNKYY-820	4
disulfide	856C:874C	N/A	disulfide	812C:821C	N/A
stalk turn	642-QTMN-645	0	extended loop from stalk	597-YWNRPIEDLSPAPREPDNIIDLPKADPDS-625	5

Extended Data Figure 5: Human sOPA1 compared to its homolog, MGM1, from *Chaetomium thermophilum*[20]. **a,** A sequence comparison between human sOPA1 and sMGM1. Regions before the S1 cleavage site are colored white, the GTPase domain is green, BSE is pink, stalk is blue, paddle is orange, and the hinges and N-terminal coiled coil are also light gray. Kinks and turns in the stalk are light blue and loops and membrane inserting regions of the paddle are light orange. **b,** An overlay of sOPA1 with MGM1, PDB ID: 6QL4 highlighting similar domain organizations. OPA1 domains are colored according to **a** and MGM1 is shown in gray. Unique regions in MGM1 and OPA1 are highlighted: the kinked-stalks, the paddle domain, and the disulfide bond in the hinge between the stalk and paddle regions. Zoomed is a 180° rotation of the paddle-tip region to highlight differences in secondary structure and domain angle. Top left, a map of sOPA1 helical assembly with a monomer colored is shown in the same orientation as the models. Helices are labeled as in the sequence alignment in Supplementary Figure 1. **c,** A 90° rotation of sOPA1 and MGM1, with a helical map of sOPA1 colored, top left. The membrane is drawn in gray to highlight increased sOPA1 insertion into the membrane. The additional Pα2 and Pα6 helices insert more deeply into the membrane in OPA1. The paddle-tip of OPA1 is also oriented more closely to the membrane whereas the MGM1 paddle-tip points away from the bilayer. The boxed region highlights membrane binding differences within the paddle-tips. **d,** A table comparing differently evolved secondary structure features and amino acid sequences between OPA1 and MGM1. Charged residues in the paddle primed to interact with the membrane are blue while aromatics are orange.

Extended Data Figure 6

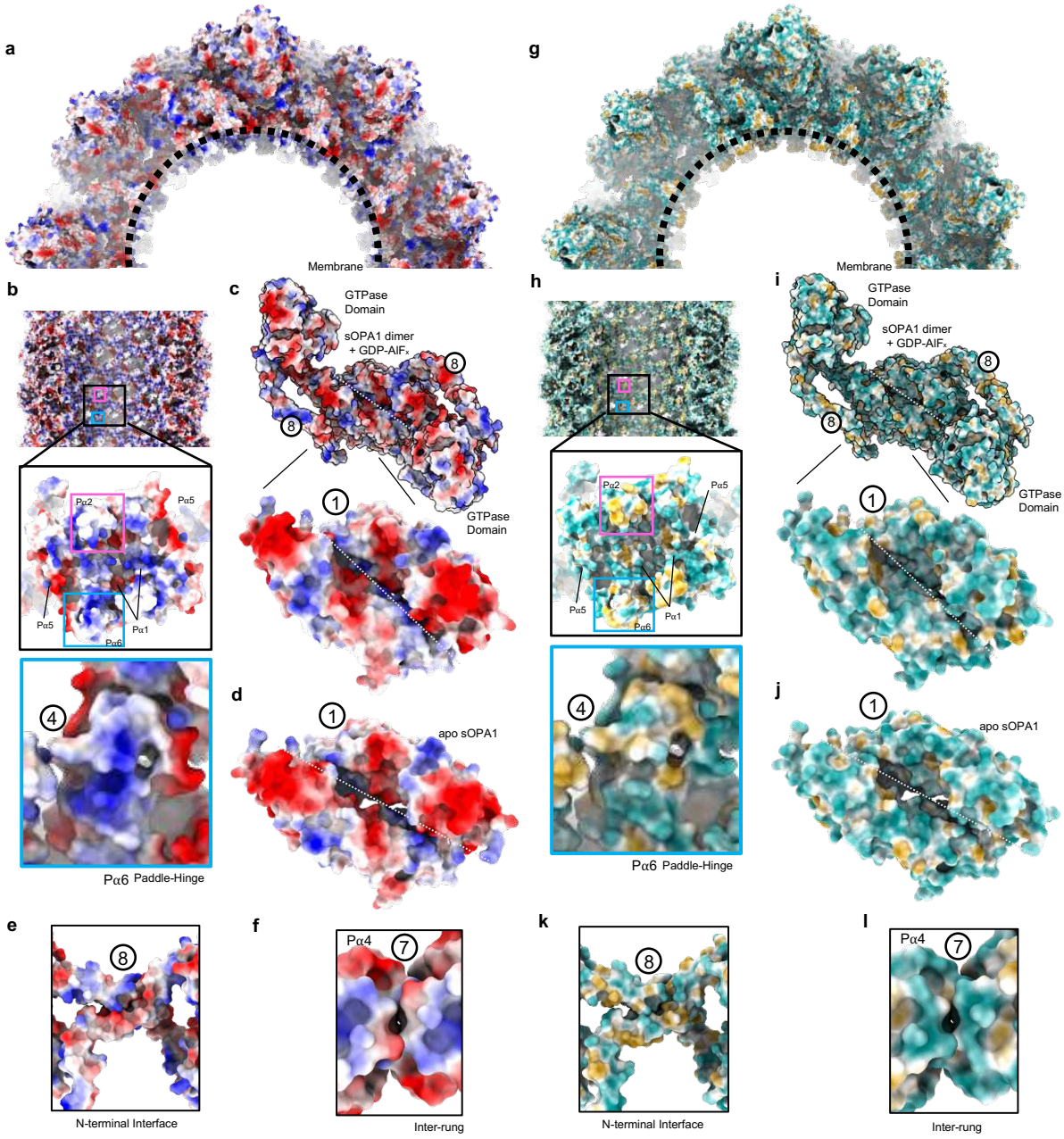

Extended Data Figure 6: Examining the electrostatic and hydrophobic distribution of the GDP-AlF$_x$ bound sOPA1 helical assembly. a, A top view of the sOPA1 helical assembly colored by Coulombic electrostatic potential (positive=blue, negative=red, neutral=white) with a dashed line marking the membrane interface. The flexible helices, Pα2 and Pα6, in the paddle-tip and -hinge line the interface with charge but become more neutral near where they would insert into the lipid tails. **b,** A clip of the full helical assembly (top) and a single sOPA1 dimer (middle) colored by electrostatic potential, focusing on the paddles on the membrane to highlight the positive charge distribution on the bilayer interface. Pink and blue boxes highlight the helices in the paddle which insert into the membrane, Pα2 and Pα6, which are in the paddle-tip and paddle-

hinge respectively. Pα1 and Pα5 are also labeled. The Blue boxed region (bottom) shows Pα6 in the context of interface-4. **c,** An sOPA1 dimer colored by electrostatic potential oriented along the side view of the helical assembly. Charge striation is particularly apparent along the dimer within the interlocked stalk interface 1 and at the site of N-terminal coiled-coil interface-8. Zoomed, the striated stalk:stalk interface-1 is highlighted. **d,** The striated apo OPA1 stalk:stalk interface-1 is shown with charge slightly out of register. **e,** A zoomed view of the electrostatic potential for the N-terminal interface 8. **f,** The inter-rung interface-7 is colored by electrostatic potential, highlighting charge dependence. **g-l,** same as in **a-f** for calculated lipophilicity**.** Coulombic electrostatic potential and molecular lipophilicity were determined using ChimeraX[40].

Extended Data Figure 7

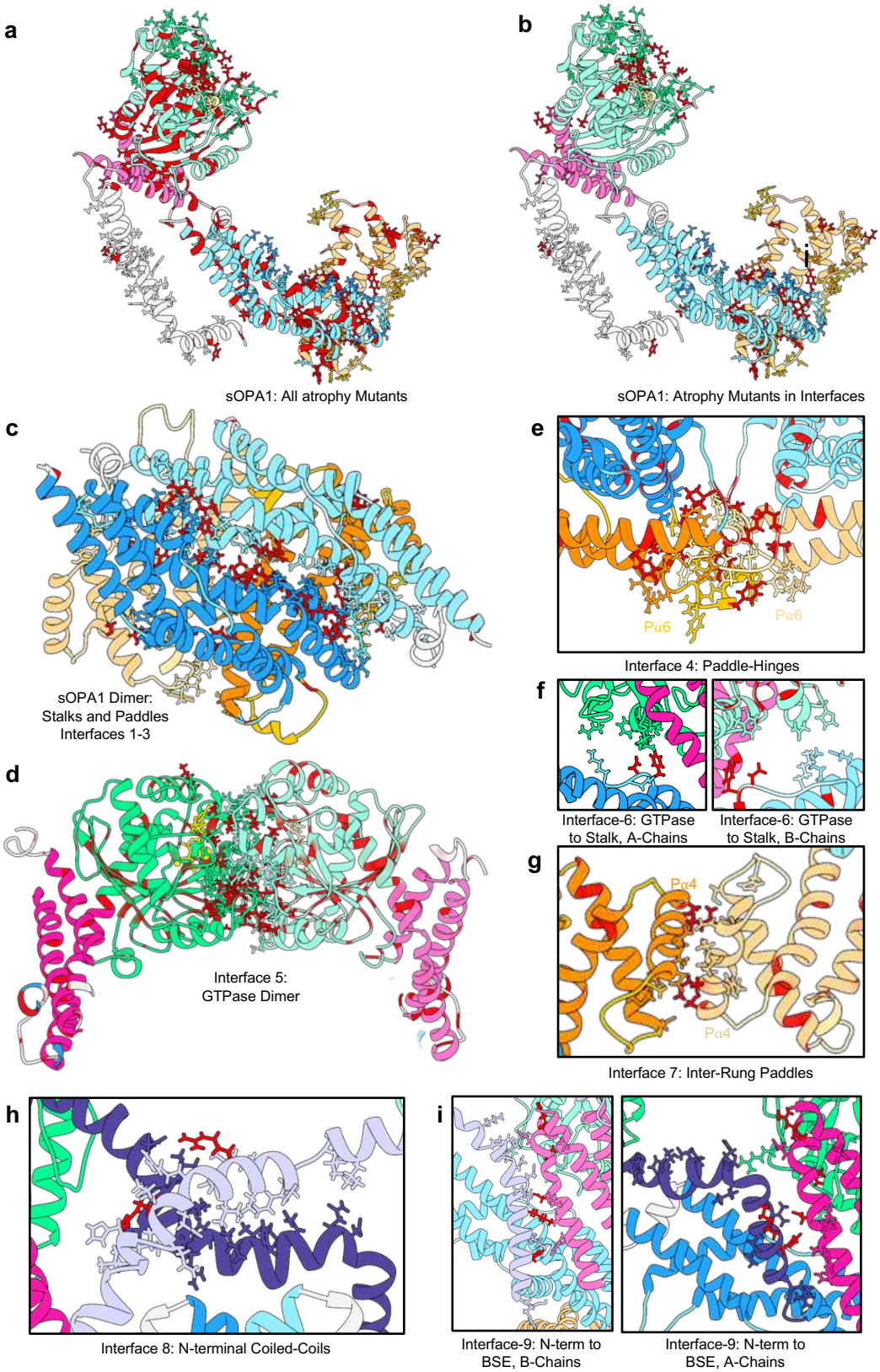

Extended Data Figure 7: A closer look at the potential residues involved in sOPA1 interfaces and the Atrophy mutants located within each interface. a, One sOPA1 A-chain is shown with all potential interfacial residues of the helical assembly shown in sticks. The Ribbon in the N-term is colored light gray, GTPase domains are colored in light green, BSEs in light pink, hinge-1 in light gray, stalks in light blue, and paddles in light orange. Sticks are colored with darker hues of the corresponding ribbon colors. All atrophy mutants are colored in red**. b,** A comparison of atrophy mutants located just within the buried interfaces. The model is colored as in A and sticks are shown for interfacial residues. Only atrophy mutants located within the interfaces are shown in red**. c,** A closer look at the total sOPA1 dimer interface between the stalks and paddles (interfaces 1-3), with sticks shown for the buried residues and atrophy mutants colored in red**. d,** A closer look at Interface-5 between GTPase domains. **e,** A view of Interface-4 between the paddle-hinges**. f,** A view of the potential GTPase domain:stalk interface (interface-6) for the A-chains (left) and B-chains (right). **g,** A view of interface-7 between inter-rung paddles**. h,** A view of interface-8 involving the N-terminal Coiled-Coil. **i,** A view of interface-9, the possible N-term to BSE interface. In all cases buried interfacial residues (determined using PDBePISA) are shown as sticks and atrophy mutants are colored in red[33].

Extended Data Figure 8

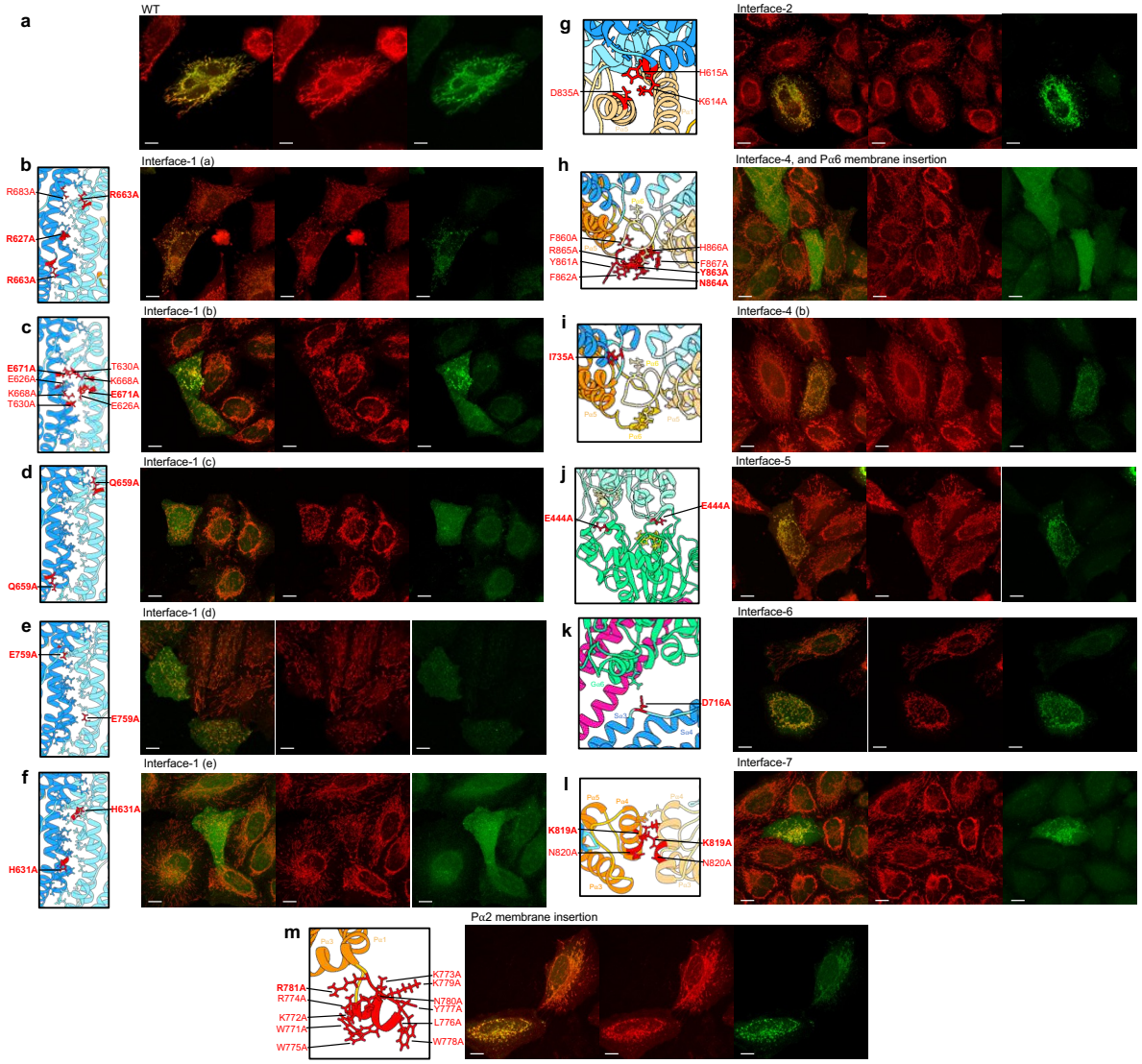

Extended Data Figure 11: Cell images examining the functional impact of interfaces between OPA1 in assembly and membrane binding in more detail. (a-m) Left, colocalization of OPA1-GFP and mitochondria stained with MitoTracker Red. Middle, MitoTracker Red stained mitochondria. Right, OPA1-GFP localization to the mitochondria. Zoomed views of the residues in each set of mutations are shown to the left of the corresponding cell images. H-bonding residues are shown in sticks. Residues mutated in the interface are colored red and labeled. **a,** WT OPA1-GFP **b,** Interface-1 (a) mutations (R627A:K663A:R683A) **c,** Interface-1 (b) mutations (E626A, T630A, K668A, E671A) **d,** Interface-1 (c) mutation (Q659A) **e,** Interface-1 (d) mutation (E679A) **f, ,** Interface-1 (e) mutation (H631A) **g,** Interface-2 mutations (K614A:H615A:D835A) **h,** Interface-4 and membrane binding Pα6 mutations (F860A:Y861A:Y862A:Y863A:Q864A:R865A:H866A:F867A) **i,** Interface-4 (b) mutation (I735A) **j,** Interface-5 mutation (E444A) **k,** Interface-7 mutations (D716A) **l,** Interface-7 mutations (K819A:N820A) **m,** Membrane binding, Pα2 mutations (W771A:K772A:K773A:R774A:W775A:L776A:Y777A:W778A:K779A:N780A:R781A). Sites which are mutated in DOA are bolded in **b**-**g**. Scale bar measures 10 μm.

Supplementary Figures, Tables and Movies

Supplementary Figure 1

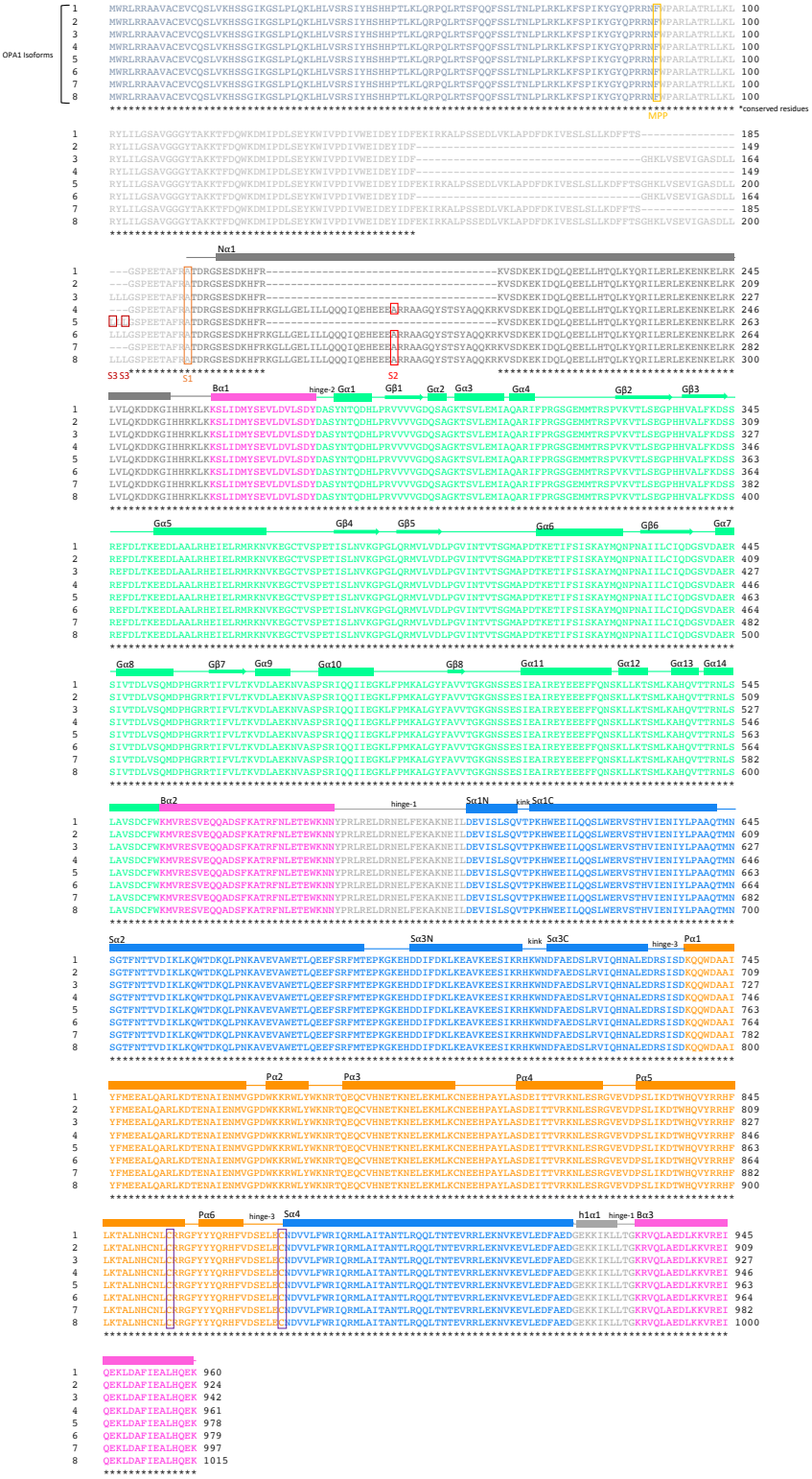

Supplementary Figure 1: Sequence alignment of the 8 OPA1 isoforms. The 8 OPA1 isoforms aligned using the Clustal Omega Multiple Sequence Alignment Tool[41]. Sequences are sourced from RefSeq (Isoform 1:NP_056375.2, Isoform 2:NP_570844.1 , Isoform 3:NP_570845.1, Isoform 4:NP_570846.1, Isoform 5:NP_570847.2, Isoform 6:NP_570848.1, Isoform 7:NP_570849.2, Isoform 8:NP_570850.2)[42]. Regions are colored by domain, where the mitochondrial targeting sequence is blue-gray, the N-terminal linker preceding S1 cleavage is light gray, the N-terminal coiled-coil following the S1 cleavage site is dark gray, BSE is pink, GTPase domain is green, stalks are blue, paddle is orange, and hinge-1 between the stalks and BSE is medium gray. The proteolytic S1, S2, and S3 cleavage sites are boxed in orange and red respectively. The cleavage site following the mitochondrial targeting sequence is boxed in yellow. Corresponding secondary structure, labeled above, are shown colored by domain above the residues, where lines mark linkers, rectangles mark helices, and arrows mark β-sheets. Asterisks below each residue mark the degree of conservation. Disulfide residues are boxed in purple.

Supplementary Figure 2

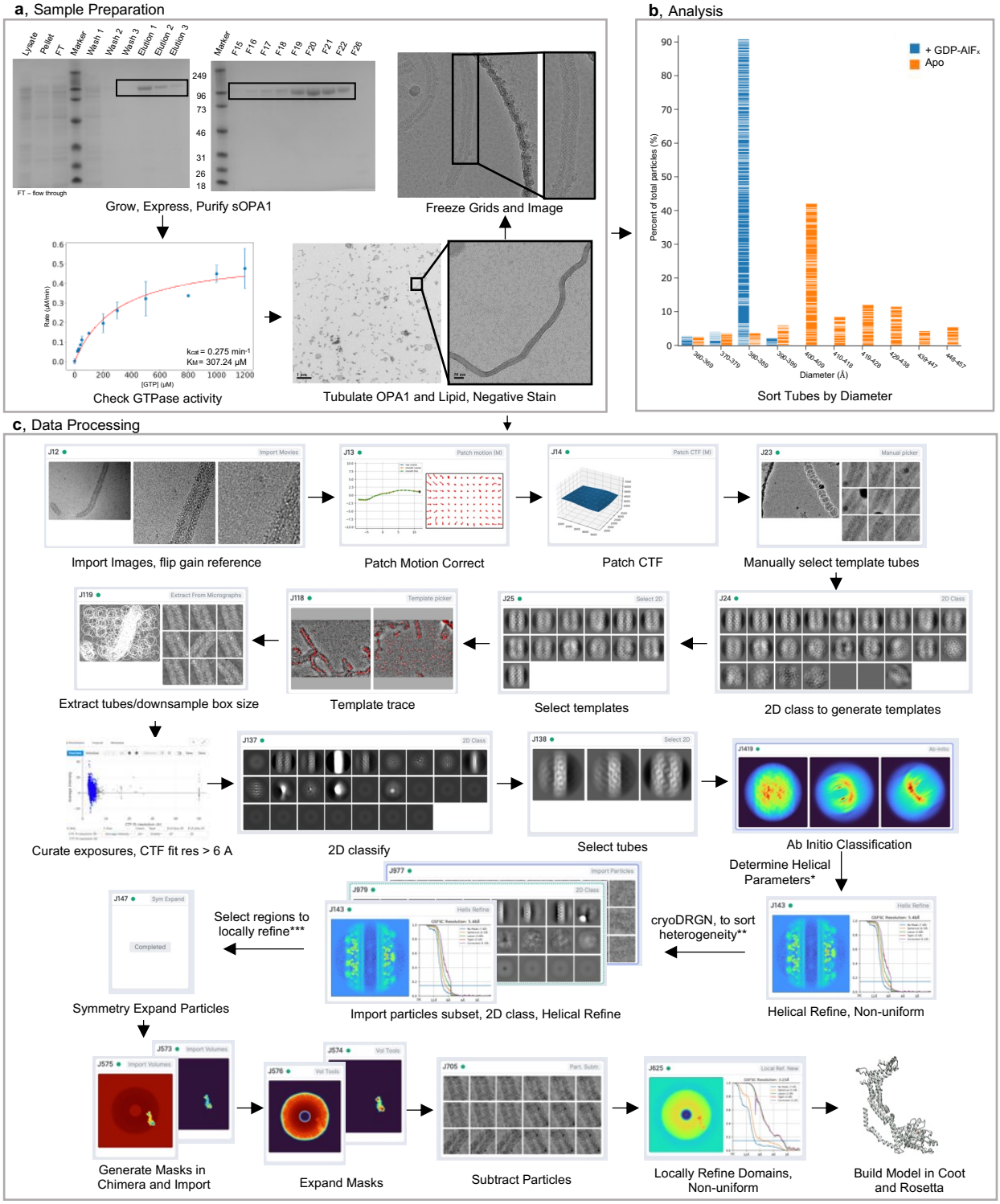

Supplementary Figure 2: cryoSPARC Workflow for determining sOPA1 helical assembly and corresponding local refinements. a, sample preparation workflow for sOPA1 purification, activity assay, and tube formation. Images for the GDP-AlF_x bound state were collected on a Titan Krios and images for the apo state were collected on a Glacios. **b,** analysis of sOPA1 tube diameter distribution for both the apo and GDP-AlF_x states. **c,** data processing. Each dataset followed a standard workflow starting with patch motion correction and patch CTF correction. Segments of the tubes were then manually selected, and 2D classified to generate templates to trace the particles, which were extracted and curated to a 6 Å CTF cutoff. These particles were 2D classified and tubes of similar identity and diameter were selected and aligned through ab initio modeling. The selected ab initio models were then refined with non-uniform helical refinement. For the GDP-AlF_x bound case, helical symmetry was determined beforehand using a combination of Fourier and real space analysis employing HELIXPLORER and RELION[43-45]. For the apo case symmetry parameters were determined in cryoSPARC. Each set of parameters was checked with the cryoSPARC helical search tool[30,46]. To examine the interfaces of each OPA1 in the assembly, local refinements were performed on various regions by first symmetry expanding the particles in the helical refinements. Then, areas of interest were determined and masks were generated in chimera, after which the masks were expanded and padded within cryoSPARC for particle subtraction before running non-uniform local refinements. The resulting maps were used to build the model of sOPA1, which was generated using COOT and Rosetta[47-49].

Supplementary Figure 3

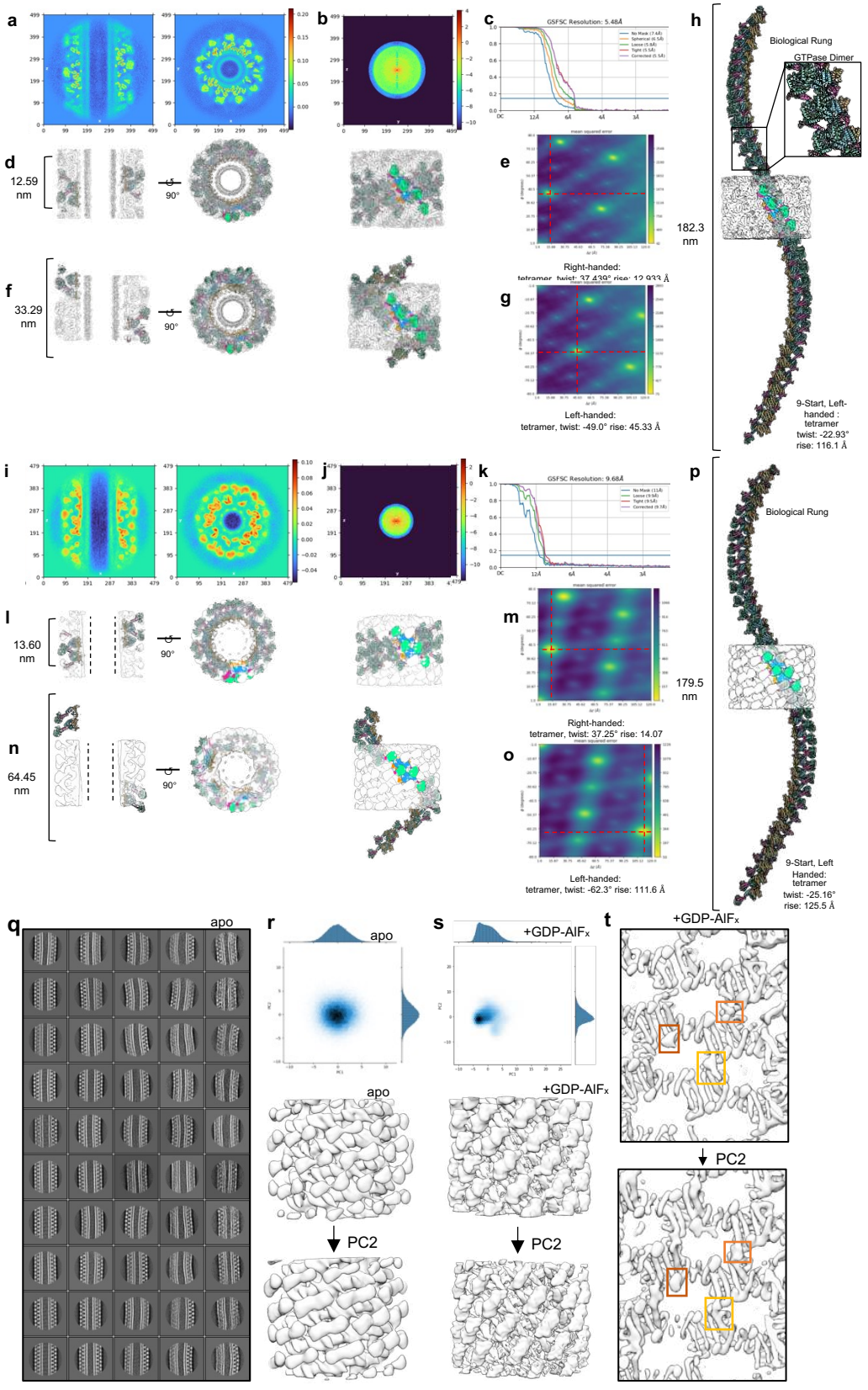

Supplementary Figure 3: Helical Refinement and Symmetry of apo and GDP-AlF$_x$ bound sOPA1 with cryoDRGN analysis. a, CryoSPARC helical projections viewed from the side and top**. b,** The power spectrum output from cryoSPARC**. c,** The FSC curves of the full helical refinement**. d,** A clip of the helix (left), solved with right-handed symmetry, then rotated 90-degrees (center) with a single turn fit into the density. A single tetramer is highlighted in each panel**.** A single turn of sOPA1 tetramers (right) is also shown fit into the density. **e,** the output lattice and solution from a helical symmetry search in cryoSPARC. **f,** a clip of the helix (left), solved with left-handed symmetry, then rotated 90-degrees (center) with a single turn fit into the density. At right, a single turn of sOPA1 tetramers is shown partially fit into the resolved map. **g,** the output lattice and solution from a helical symmetry search in cryoSPARC. **h,** A single turn of the 9-start sOPA1 helix is shown partially fit into the resolved map with a single tetramer unit highlighted. Inset shows the intra-rung GTPase dimer (interface-5)**. i-p**, same as in **a-h** for the apo helical assembly**. q,** 2D classifications of the apo sOPA1 helical assembly highlight largescale flexibility and tube curvature as well as variability in diameter**. r,** Principal component plot (top) of the apo assembly from cryoDRGN. Start (center) and end (bottom) points of principle component 2 (PC2) are shown for the apo helix. **s,** same as in **r** but for the GDP-AlF$_x$ state. **t,** Zoomed slices displaying just the paddle domain insertion into the membrane from the first and final volume of the GDP-AlF$_x$ bound helix as seen in Y. Boxed regions focus on the paddle-tip and -hinge helices, Pα2 and Pα6.

Supplementary Table 1

OPA1 Interfaces	Nucleotide Bound				Nucleotide-Free
	Average Buried Surface Area (Å2)	Residues which H-bond/Salt Bridges	Buried Interface Residues (A-chain)	Buried Interface Residues (B-chain)	Buried Surface Area (Å2)
sOPA1 Dimer (Stalks and Paddles)	1429	K614 (A):D835 (B), **R627 (A)**:E671 (B), N635 (A):E679 (B), **K663 (A)**:E706 (B), K668 (A):E675 (B), **R683 (A)**:E634 (B), E679 (A):N635 (B), E702 (A):**Q659 (B)**, E706 (A):K663 (B), E675 (A):Q664 (B), **E671 (A)**:K668 (B), K668 (A):**E671 (B)**, H615 (A):D835 (B), E626 (A):**R755 (B)**, D835 (A):K614 (B), Y808 (A):K689 (B)	**T612**, K614, H615, E618, Q622, E626, **R627**, T630, **H631**, E634, N635, L638, P639, N642, T643, T648, I655, **K656**, **Q659**, **K663**, Q664, K668, **E671**, E675, E679, S682, **R683**, T686, **E687**, P688, G690, K691, E702, K705, E706, **I709**, K710, K738, **F747**, E750, **R755**, K757, D758, N761, A762, H788, E804, P806, A807, Y808, A810, **S831**, **L832**, D835, H838, Q839, **Y841**, Y861	**T612**, K614, H615, E618, Q622, E626, **R627**, S629, T630, **H631**, E634, N635, L638, P639, N642, M644, I655, **K656**, **Q659**, **K663**, Q664, K668, **E671**, E675, Q678, E679, **R683**, T686, **E687**, P688, K689, G690, K691, E692, E702, K705, E706, K710, E750, **R755**, K757, D758, N761, **N765**, L776, Y777, W778, K779, N802, E804, P806, A807, Y808, **S831**, D835, H838, Q839	1059
Interface1:Interlocked Stalks	805	**R627 (A)**:E671 (B), N635 (A):E679 (B), **K663 (A)**:E706 (B), K668 (A):E675 (B), **R683 (A)**:E634 (B), E679 (A):N635 (B), E702 (A):**Q659 (B)**, E706 (A):K663 (B), E675 (A):Q664 (B), **E671 (A)**:K668 (B), K668 (A):**E671 (B)**	E626, **R627**, T630, **H631**, E634, N635, L638, P639, N642, T643, T648, I655, **K656**, **Q659**, K663, Q664, K668, **E671**, E675, E679, S682, **R683**, T686, **E687**, P688, G690, K691, E702, K705, E706, **I709**, K710	E626, **R627**, S629, T630, **H631**, E634, N635, L638, P639, N642, M644, I655, **K656**, **Q659**, K663, Q664, K668, **E671**, E675, Q678, E679, **R683**, T686, **E687**, K689, G690, E702, K705, E706, K710	458
Interface-2: A-chain Stalk to B-chain Paddle	263	K614 (A):D835 (B), H615 (A):D835 (B), E626 (A):**R755 (B)**	**T612**, K614, H615, E618, Q622, E626, **R683**, **E687**, P688, K689, G690, K691	**R755**, D758, N802, E804, P806, A807, Y808, **S831**, D835, H838, Q839, R842	357
Interface-2: B-chain Stalk to A-chain Paddle	306	D835 (A):K614 (B), Y808 (A):K689 (B)	R755, D758, A762, H788, E804, P806, A807, Y808, A810, **S831**, **L832**, D835, H838, Q839, **Y841**	**T612**, K614, H615, E618, Q622, E626, **R683**, P688, K689, G690, K691, E692	252
Interface-3: Paddle:Paddle	120	none	K738. **F747**, E750, K757, N761, Y861	E750, K757, N761, **N765**, L776, Y777, W778, K779	10
sOPA1 Assembly beyond the Dimer					
Interface-4: Paddle-Hinges	878	H866 (A):R858 (B), D869 (A):K738 (B), F867 (A):K738 (B), **I735 (A)**:R865 (B), **Y863 (A)**:E871 (B), K738 (A):D869 (B)	**I735**, **S736**, K738, W741, D742, **I745**, **Y746**, **C856**, R857, R858, G859, F860, Y861, **Y863**, R865, H866, F867, V868, D869, S870, **L872**, E873, C874, N875, V877	**S736**, D737, K738, L855, R857, R858, G859, F860, Y862, **Y863**, Q864, R865, H866, F867, V868, D869, S870, E871, **L872**, E873	396
Interface-5: GTPase Dimer	1713	S408 (A):K489 (B), **R445 (A)**:**R445 (B)**, R481 (A):G409 (B), **K505 (A)**:N475 (B), D442 (A):N297 (B), **D450 (A)**:T405 (B), K489 (A):S408 (B), **R445 (A)**: **D296 (B)**, E450 (A):K415 (B), **D296 (A)**:**R445 (B)**, E320 (A):R481 (B)	**D296**, Q297, **A299**, **G317**, S318, G319, E320, M321, **T376**, **V402**, I403, **N404**, **T405**, V406, T407, S408, M410, Q437, D438, S440, V441, D442, **A443**, **E444**, **R445**, **S446**, I447, **T449**, **D450**, **K468**, **D470**, **L471**, K474, N475, V476, A477, S478, P479, S480, R481, Q484, I485, **G488**, K489, L490, F491, P492, **K505**, G506, N507	**D296**, Q297, **S298**, S318, G319, E320, M321, R324, **V402**, I403, **N404**, **T405**, V406, T407, S408, **G409**, **M410**, K415, D438, S440, V441, D442, **A443**, **E444**, **R445**, **S446**, I447, **T449**, **D450**, **K468**, **D470**, **L471**, E473, K474, N475, V476, A477, S478, S480, R481, Q484, K489, L490, P492, **K505**, G506, N507	none
Interface-6: GTPase to Stalk Contact (A-chains)	110	**D716 (A)**:K423 (B)	K713, N715, **D716**, **F717**	Y282, F419, S420, K423, Q427, Q454	none
Interface-6: GTPase to Stalk Contact (B-chains)	90	K713 (A):Q454 (B)	F419, S420, K434, N437, N454, H458	K713, **D716**, **F717**, K908, E912	none
Interface-7: Inter-Rung Paddles	335	**K819 (A)**:E813 (B), N820 (A): N820 (B), E813 (A): K819 (B), K819 (A): D812 (B), D812 (A):K819 (B)	M798, C801, A810, D812, E813, T815, T816, **K819**, N820, **S823**	C801, H805, D812, E813, T815, T816, R818, **K819**, N820, **S823**	308
Interface-8: N-term Coiled-Coil	780	R235 (A):L223 (B), E220 (A):N240 (B), E221 (A):K241 (B), E239 (A): R231 (B), H224 (A):E237 (B), E239 (A): **R235 (B)**	D216, Q217, E220, E221, H224, T225, K228, Y229, R231, I232, E234, **R235**, L236, E237, E239	S200, D203, K204, L223, H224, Q226, L227, K228, Q230, R231, L233, Q234, **R235**, E237, K238, N240, K241, L243, L246	none
Interface-9: NtoBSE	348	Q217 (A):Q562 (B)	R198, **H205**, K208, V209, **K212**, **E213**, I215, D216, Q217, E220, E221, H224, T225, K228	H287, **N430**, R460, **R557**, E558, S559, E561, Q562, **D565**, S566, K568, A569, F572, N573, E954, K690	246 (not fully resolved)

Supplementary Table 1: Interfaces of OPA1 helical assembly. Buried surface area and residues for each interface as identified by the server PDBePISA[33] sites with mutations identified in DOA are bolded.

Supplementary Table 2

Data collection and processing	OPA1 GDP-AlFx:dimer	OPA1 GDP-AlFx:tetramer	OPA1 GDP-AlFx:9-dimers	OPA1 apo:dimer	OPA1 apo:tetramer	OPA1 apo:9-dimers
Microscope	Titan Krios	Titan Krios	Titan Krios	Glacios	Glacios	Glacios
Magnification of K3 data	105,000x	105,000x	105,000x	36,000x	36,000x	36,000x
Voltage (kV)	300	300	300	200	200	200
Electron exposure (e–/Å ^{2})	60	60	60	24.86	24.86	24.86
Defocus range (-μm)	0.3 to 2.4	0.3 to 2.4	0.3 to 2.4	0.6 to 2.4	0.6 to 2.4	0.6 to 2.4
spherical abberation (mm)	2.7	2.7	2.7	2.7	2.7	2.7
Pixel size (Å)	1.2018	1.2018	1.2018	1.2518	1.2518	1.2518
Symmetry imposed	Helical	Helical	Helical	Helical	Helical	Helical
total number of micrographs (no.)	6,319	6,319	6,319	2,830	2,830	2,830
Initial particle images (no.)	2,151,757	2,151,757	2,151,757	1,008,912	1,008,912	1,008,912
Final particle images helical (no.)	598,503	598,503	598,503	88,155	88,155	88,155
Final particle images local (no.)	1,795,509	1,795,509	1,795,509	352,620	352,620	352,620
Box Size (pixels)	500	500	500	480	480	480
Map resolution helical (Å) (initial, N-term)	5.48, 6.51	5.48, 6.51	5.48, 6.51	9.68	9.68	9.68
Map resolution helical Z-clipped (Å)	3.86	3.86	3.86	5.80	5.80	5.80
Map resolution (Å)	3-3.4	3-3.4	3-3.4	5.5-6.5	5.5-6.5	5.5-6.5
FSC threshold	0.143	0.143	0.143	0.143	0.143	0.143
Helical Parameters						
Inner Diameter (nm)	9.4	9.4	9.4	9.5	9.5	9.5
Outer Diameter (nm)	38.2	38.2	38.2	40.5	40.5	40.5
Pitch (Å)	125.9	125.9	125.9	136.0	136.0	136.0
Rise (Å)	12.933	12.933	12.933	14.07	14.07	14.07
Twist (°)	37.439	37.439	37.439	37.25	37.25	37.25
Units per turn (tetramers)	9.62	9.62	9.62	9.66	9.66	9.66
Start (no.)	1	1	1	1	1	1
Refinement						
Initial model hybridized, Alphafold model	AF-O60313-F1	AF-O60313-F1	AF-O60313-F1	AF-O60313-F1	AF-O60313-F1	AF-O60313-F1
Chains (no.)	2	4	18	2	4	18
Model resolution (Å)	4.6	6.9	6.9	9.9	-	-
FSC threshold	0.143	0.143	0.143	0.143	-	-
Model composition						
Non-hydrogen atoms	12,604	25,208	113,436	12,534	25,068	112,806
Protein residues	1,532	3,064	13,788	1,532	3,064	13,788
Ligands	8	16	72	0	0	0
B-factor						
Protein (Å $^{2)}$	95.76	95.76	95.76	87.91	87.91	87.91
GDP (Å ^{2})	8.03	8.03	8.03	-	-	-
ligands (Å ^{2})	15.45	15.45	15.45	-	-	-
Validation						
MolProbity Score	1.38	1.46	1.53	1.44	1.44	1.54
Clashscore	6.87	8.49	10.1	7.5	7.94	10.59
Ramachandran plot						
Favored (%)	98.3	98.3	98.3	98.56	98.56	98.56
Allowed (%)	1.7	1.7	1.7	1.44	1.44	1.44
Disallowed (%)	0	0	0	0	0	0
Rotamers outliers (%)	0.04	0.04	0.04	0.07	0.07	0.07
Cβ outliers (%)	0	0	0	0	0	0
R.M.S. deviations						
Bond Length (Å)	0.021 (0.16%)	0.021 (0.16%)	0.021 (0.16%)	0.018 (0.13%)	0.018 (0.13%)	0.018 (0.13%)
Bond Length (°)	1.772 (0.21%)	1.772 (0.21%)	1.772 (0.21%)	1.726 (0.19%)	1.726 (0.19%)	1.726 (0.19%)
Peptide plane (%)						
Cis proline/general	0/0.01	0/0.01	0/0.01	0/0	0/0	0/0
twisted proline/general	0/0	0/0	0/0	0/0	0/0	0/0
CaBLAM outliers (%)	0.92	0.92	0.92	0.72	0.72	0.72

Supplementary Table 2: CryoEM data collection, refinement, and validation statistics.

Supplementary Movie 1: Morphs between the Models of the Apo and Nucleotide bound state of sOPA1

Supplementary Movie 2: Transition of the helical assembly with and without nucleotide from cryoDRN

Methods

Expression and purification of the sOPA1 construct

The short OPA1, isoform 1 was expressed and purified with modifications from plasmid and protocols provided by David Chan. sOPA1 (residues 195-960) was expressed in BL21-DE3(RIL) cells using a pET28a vector with an N-terminal 6xHIS tag. Cells were grown in terrific broth (TB) media to an OD_{600} of 1.2-1.3. Cells were then cold shocked for 30 minutes at 4°C and induced with 0.5 mM IPTG. After an overnight incubation at 16°C with 300 rpm shaking, cells were harvested by centrifugation.

sOPA1 was purified using TALON metal affinity resin (Takara Bio) and size exclusion chromatography (SEC). In brief, pelleted cells were resuspended in lysis buffer (20 mM Tris pH 8, 500 mM NaCl, 5 mM Imidazole) with the addition of 1 mg/mL of lysozyme, 0.01% DNAse, and a protease inhibitor tablet (EDTA free, Roche), incubated for 1 hour at 4°C, and lysed via probe sonication (1 minute process time, 1 second on, 5 seconds off at 90% amplitude). Cell debris was pelleted via ultracentrifugation at 230,000 xg for 1 hour at 4°C. Clarified lysate was transferred to TALON resin and treated with wash buffer (20 mM Tris pH 8, 500 mM NaCl, 20 mM imidazole) and elution buffer (20 mM Tris pH 8, 500 mM NaCl, 250 mM imidazole). Fractions containing sOPA1 were pooled, concentrated, and washed into SEC buffer (20 mM Tris pH 8, 300 mM NaCl, 1 mM DTT) using a 30 kDa AmiconUltra concentrator. Protein precipitation was pelleted by centrifugation at 13,000 xg for 1 minute, and the sample was run over an S650 size exclusion column (BioRad). After examination by SDS-PAGE, fractions containing sOPA1 were pooled, exchanged into HCB150 buffer (20 mM HEPES, pH 7.2, 150 mM KCl, 1 mM $MgCl_2$, 2 mM EGTA, 1 mM DTT) and concentrated to ~2mg/mL. Protein was quantified by absorbance at 280 nm, flash frozen in liquid nitrogen, and stored at -80°C.

GTPase Assay

Basal GTP hydrolysis of sOPA1 was measured using the colorimetric malachite-green assay described by Leonard et al[50]. Reactions were performed at 37°C using sOPA1 at 2 μM in HCB150 buffer (20 mM HEPES, pH 7.2, 150 mM KCl, 1 mM $MgCl_2$, 2 mM EGTA, 1 mM DTT) in the presence of GTP (Jena Biosciences). Using Plotly and python, the data were fit to the equation, $\nu = (k_{cat}\,[E_0]\,[S])/(K_M+[S])$, where ν is the initial rate of GTP hydrolysis, E_0 is the concentration of the sOPA1 enzyme, S is the concentration of the GTP substrate, K_M is the Michaelis constant, and k_{cat} is the turnover number.

Liposome Preparation

Large unilamellar vesicles composed of 75% 1,2-dioleoyl-sn-glycero-3-phospho-L-serine (DOPS) and 25% 18:1 cardiolipin (CL) (1',3'-bis[1,2-dioleoyl-sn-glycero-3-phospho]-glycerol) were prepared via extrusion (Avanti Polar Lipids). Vesicles were prepared by solubilizing the lipid mixture in chloroform then drying with rotation in a warm water bath under argon. Mixtures were further dried under in a desiccator under vacuum overnight. Lipid film was then solubilized to 0.8 mg/mL in a warm water bath, with occasional vortexing, into HCB150 buffer (20 mM HEPES, pH 7.2, 150 mM KCl, 1 mM $MgCl_2$, 2 mM EGTA, 1 mM DTT). 0.8 μm LUVs were then generated via extrusion using an extruder by Avanti polar lipid using a 0.8 μm pore size polycarbonate membrane (Avanti).

sOPA1 Lipid Tubulation

sOPA1 and a lipid mixture, diluted to 0.4 mg/mL of 75:25 DOPS:CL liposomes in HCB150 buffer (20 mM HEPES, pH 7.2, 150 mM KCl, 1 mM $MgCl_2$, 2 mM EGTA, 0.1 mM DTT) containing 10 % ethylene glycol to a final concentration of a 1.4 mg/mL protein to 0.12 mg/mL ratio were combined, briefly vortexed, then immediately bath sonicated for 5 minutes. Post-

sonication tubes were incubated between 25-60 minutes. For tubes in the presence of nucleotide, GDP-AlF_x was then added to a final concentration of 1 mM and allowed to incubate for another 10-15 minutes. A GDP-AlF_x stock was generated by combining GDP, $AlCl_3$, and NaF to final concentrations of 10 mM, 60 mM, and 300 mM, prepared within the 10 minutes preceding addition to sOPA1:lipid tubes.

Negative Stain

sOPA1:lipid mixtures were loaded onto carbon-coated, 15 second glow discharged, nickel formvar (FCF400 Ni-NA**)** grids and incubated for 1 minute, followed by staining with 1% uranyl acetate. Grids were visualized on a FEI Technai 12, as part of the NIDDK core facility.

Plunge Freezing

3 µL of sOPA1:lipid tubes were aliquoted onto carbon coated, 90 second glow discharged, C-flat gold grids (CF-1.2/1.3-4Au50), incubated for 30 seconds, blotted with filter paper for 3 seconds (4°C with 95% humidity) and then plunged into liquid ethane using a Leica EM Grid Plunger (Leica Microsystems). Vitrified grids were stored in liquid nitrogen before examination using cryo-electron microscopy (cryoEM).

CryoEM

Samples were screened a TF20 microscope (FEI) at 200 kV at a 29,000x magnification, with a nominal defocus range of 1.5 to 3.0 µm using a K2 summit camera (Gatan) in counting mode. High-resolution images of OPA1 lipid tubes in the presence of GDP-AlF_x were recorded on a Titan Krios G3 microscope (Thermo-Fisher) operating at 300 kV on a Gatan K3 camera. 6,319 images were collected at a magnification of 105,000x with calibrated pixel size of 0.415 Å, nominal defocus range of 0.3 to 2.4 µm, 24 frames, and 60 e-/Å2 electron exposure per movie. Images of OPA1 lipid tubes in the apo state were recorded on a Glacios cryo-TEM microscope (Thermo-Fisher) operating at 200 kV on a Gatan K3 camera. 2,830 images were collected at a magnification of 36,000x calibrated pixel size 0.58 Å, nominal defocus range 0.6 to 2.4 µm, 22 frames, and 24.86 e-/Å2 electron exposure per movie.

Preliminary CryoEM Processing and determination of helical parameters in RELION 3.1, FIJI, and HELIXPLORER

Preliminary micrographs from the FEI TF20 of sOPA1:lipid tubes with GDP-AlF_x were motion corrected and dose-weighted with MotionCor2 in RELION 3.1[44,51]. CTF estimation was determined in RELION 3.1 using Ctffind4[52]. Particle selection was performed manually in RELION 3.1[44,45]. Extracted particles were used to generate initial 2D reference classes for real space analysis of helical parameters. Motion corrected particles generated in RELION 3.1 were also used to generate stacks of averaged power spectrum for Fourier Bessel analysis in FIJI[53,54]. Suspected helical parameters were then input into HELIXPLORER (Esterozi, L, http://rico.ibs.fr/helixplorer/)[55] in order to determine a range of potential solutions[53].

CryoEM Processing in cryoSPARC 3.2.0 and cryoDRGN

Final images of sOPA1:lipid tubes in the GDP-AlF_x or apo state were processed using cryoSPARC v3.2.0[30,46]. Images were gain corrected, motion-corrected, binned, and dose-weighted using Patch Motion Correction in cryoSPARC[30,46]. CTF estimation was determined using Path CTF estimation in cryoSPARC[30,46]. Particle selection was performed by generating a template, by manually selecting a subset of desired sOPA1 tubes, 2D classifying, then template tracing and extracting particles with a 1.2018 Å/pixel size and a 500-pixel box size, for the GDP-AlF_x bound dataset, and a 1.2518 Å/pixel size and a 480-pixel box size for the apo dataset. Selected particles were then examined and filtered according to a 6 Å CTF resolution using the curate exposures job. Particles were then pruned using 1 round of 2D classification. Initial tube alignment was performed

using the *ab initio* reconstruction job and helical maps were generated using the helical refinement (Beta) pipeline. Suspected helical symmetry, determined above, was cross-examined using the symmetry search tool in cryoSPARC[46]. Due to heterogeneity in tube diameter for apo OPA1 images, multiple rounds of iterative 2D classification, selection, and helical refinement were performed to produce the final helical map. After generating an initial helical map with a z-clipped region of 0.518, a local refinement was performed to focus in on a 30% z-clipped region to better compare to maps generated in RELION 3.1[43-45]. Local Refinement on sOPA1 was performed using the Local Refine (Beta) pipeline in cryoSPARC using masks generated in Chimera[30,46]. Local resolution maps were also generated in cryoSPARC[30,46].

To sort heterogeneity of the apo sample, a subset of particles were selected from outputs in cryoDRGN[31], which were re-imported and refined using cryoSPARC's helical and local refine Beta pipelines[30,46].

Maps generated in cryoSPARC were post-processed using deepEMhancer[56].

Diameter Measurements

The diameter distribution of sOPA1 tubes in apo and GDP-AlF_x bound state was determined using 2D classifications in cryoSPARC. Particles were divided into ~500 2D classes per state. The tube diameter of each class was measured using Fiji. The resulting stacked bar chart was created using Plotly[57].

Model Building and Refinement

Initial fitting of sOPA1-MGD (GTPase dimer reference) into cryoEM helical maps was done manually in UCSF Chimera[40] with the PDB:6JTG[29]. To perform local refinements in cryoSPARC, initial models were then extended from the sOPA1-MGD, de novo, using COOT 0.9[47]. The initial model was iteratively refined in COOT as the map resolution improved and features became more apparent[47]. Upon the release of the AlphaFold database, the initial model was hybridized with the AlphaFold OPA1 structure, AF-O60313-F1, in COOT 0.9 to produce a model for refinement[47,58]. Model refinement was performed using Rosetta and COOT then assessed using MolProbity and Phenix[47-49,59,60]. The cryo-EM data collection, final refinement, and validation statistics for the model are presented in Supplementary Table 2. Structural analysis, measurements and figures were prepared in Chimera and ChimeraX[40]. Interfacial areas were calculated using the PDBePISA server[33].

Summary of Helical Assemblies

Visually, the biological twist and rise of the densely packed rungs of both sOPA1 assemblies are left-handed (Supplementary Fig. 3h,p). However, we chose to define the helical parameters along the opposing lattice in right-handed coordinates which allowed us to minimize the rise and pitch of a full turn. This maximized the number of units for a given box size, which had computationally limited our attempts at left-handed solutions[43,46].

In the right-handed solution space, both assemblies are 1-start, with a pitch of 12.59 nm (Supplementary Data Fig. 3a-d) in the GDP-AlF_x bound map has and 13.60 nm in the apo map (Supplementary Data Fig. 3i-l). The GDP-AlF_x bound assembly had a twist of 37.439° and rise of 12.933 Å (Supplementary Data Fig. 3e) while the apo assembly instead had a twist of 37.25° and rise of 14.07 Å (Supplementary Data Fig. 3p). The helical maps were z-clipped in cryoSPARC to 50% of the full map (Extended Data Fig. 1c-d)[30,46]. The flexibility and continuous heterogeneity were examined and minimized for the apo assembly using cryoDRGN (Supplementary Data Fig. 3q-t and Extended Data Movie 2)[31].

An alternative minimal left-handed lattice of the GDP-AlF_x bound would be a 4-start helix with a pitch of 33.29 nm (Supplementary Data Fig. 3f), compared to an 8-start helix with a pitch

of 64.45 nm for the apo assembly (Supplementary Data Fig. 3n). The left-handed GDP-AlF_x bound assembly has a twist of -49.0° and rise of 45.33 Å (Supplementary Data Fig. 3g) compared to a twist of 62.3° and rise of 111.6 Å for the apo assembly (Supplementary Data Fig. 3o).

The apparent biological rung of the helical assembly is based on visual packing. The biological assemblies form left-handed, 9-start helical lattices of ~16 tetrameric dimers-of-dimers. A full turn for the GDP-AlF_x bound map has a pitch of 182.3 nm (Supplementary Data Fig. 3h) and the apo case has a pitch of 179.5 nm (Supplementary Data Fig. 3p). The GDP-AlF_x bound helix has a twist of -22.93° and rise of 116.1 Å (Supplementary Data Fig. 3h) while the apo helix has a twist of -25.16° and rise of 125.5 Å (Supplementary Data Fig. 3p).

Mutations of full length OPA1 for imaging

Full length *human OPA1, isoform 1* cDNA was obtained, courtesy of David Chan, through Addgene (#70173). The OPA1 cDNA sequence was then ligated into a pEGFP-N1 vector (Clonetech), attached through an 8 amino acid linker, GLALPVAT, to an adjoining GFP fluorescent protein tag using the In-Fusion HD Cloning kit (Clonetech, 638911) following manufacturer's instructions. Alanine mutations were introduced into the FL OPA1-GFP sequence as single mutations by site-directed mutagenesis using the Quikchange II XL Site-Directed Mutagenesis Kit following manufacturer's instructions for the following mutants: E444A (Interface-5), Q659A (Interface-1 (c)), E679A (Interface-1 (d)), H631A (Interface-1 (e)), I735A (Interface-4 (b)). Multiple alanine mutations were introduced into the FL OPA1-GFP sequence using the QuikChange Lightning Multi Site-Directed Mutagenesis Kit (Agilent Technologies) following manufacturer's instructions for the following mutants: R627A:K663A:R683A (Interface-1 (a)), E626A:T630A:K668A:E671A (Interface-1 (b)), K819A:N820A (Interface-7), and K614A:H615A:D835A (Interface-2), D716A (Interface-6). Sequential alanine mutations were introduced into the FL OPA1-GFP sequence as nucleotide substitutions using the Q5® Site-Directed Mutagenesis Kit (New England Biolabs), for mutants: W771A:K772A:K773A:R774A:W775A:L776A:Y777A:W778A:K779A:N780A:R781A (Pα2) and F860A:Y861A:Y862A:Y863A:Q864A:R865A:H866A:F867A (Pα6 and Interface-4). Primers were synthesized by Eurofins. Plasmid concentration and purity was checked using a NanoDrop (Thermo Scientific). The coding sequences were verified by Sanger sequencing (Psomagen) and the integrity of the full-length plasmids were further verified by nanopore sequencing (Plasmidsaurus).

Imaging using Mitochondrial fragmentation using light microscopy

Hela-M cells were cultured in DMEM (Gibco by Life Technologies) with 10% heat-inactivated FBS (Gibco by Life Technologies) and 1% Antibiotic-Antimycotic solution (Gibco by Life Technologies) and were maintained at 37°C in a humidified 5% CO_2 Incubator. Cells were plated in glass-bottom 8- or 4-well chambers (Cellvis) coated with Fibronectin (10 ng/ml; Gibco by Life Technologies) and then transfected using Lipofectamine-2000 according to the manufacturer's instructions (Invitrogen by Thermo Fisher Scientific).

Transfected cells were identified by the OPA1-GFP signal above the background. Mitochondrial morphology was visualized using the red MitoTracker™ signal and then categorized as "fragmented", "intermediate", or "filamentous". The data are representative of at least three transfection sample repetitions. Categorization was performed using Zeiss ZEN 3.0 and FIJI software.

Methods References

40 Pettersen, E. F. *et al.* UCSF ChimeraX: Structure visualization for researchers, educators, and developers. *Protein Sci* **30**, 70-82, doi:10.1002/pro.3943 (2021).

41 Madeira, F. *et al.* Search and sequence analysis tools services from EMBL-EBI in 2022. *Nucleic Acids Res*, gkac240, doi:10.1093/nar/gkac240 (2022).

42 O'Leary, N. A. *et al.* Reference sequence (RefSeq) database at NCBI: current status, taxonomic expansion, and functional annotation. *Nucleic Acids Res* **44**, D733-745, doi:10.1093/nar/gkv1189 (2016).

43 He, S. & Scheres, S. H. W. Helical reconstruction in RELION. *Journal of Structural Biology* **198**, 163-176, doi:https://doi.org/10.1016/j.jsb.2017.02.003 (2017).

44 Zivanov, J. *et al.* New tools for automated high-resolution cryo-EM structure determination in RELION-3. *Elife* **7**, doi:10.7554/eLife.42166 (2018).

45 Zivanov, J., Nakane, T. & Scheres, S. H. W. Estimation of high-order aberrations and anisotropic magnification from cryo-EM data sets in RELION-3.1. *IUCrJ* **7**, 253-267, doi:10.1107/s2052252520000081 (2020).

46 Punjani, A., Rubinstein, J. L., Fleet, D. J. & Brubaker, M. A. cryoSPARC: algorithms for rapid unsupervised cryo-EM structure determination. *Nature Methods* **14**, 290-296, doi:10.1038/nmeth.4169 (2017).

47 Emsley, P., Lohkamp, B., Scott, W. G. & Cowtan, K. Features and development of Coot. *Acta Crystallogr D Biol Crystallogr* **66**, 486-501, doi:10.1107/s0907444910007493 (2010).

48 DiMaio, F. Advances in Rosetta structure prediction for difficult molecular-replacement problems. *Acta Crystallogr D Biol Crystallogr* **69**, 2202-2208, doi:10.1107/s0907444913023305 (2013).

49 Wang, R. Y. *et al.* Automated structure refinement of macromolecular assemblies from cryo-EM maps using Rosetta. *Elife* **5**, doi:10.7554/eLife.17219 (2016).

50 Leonard, M., Song, B. D., Ramachandran, R. & Schmid, S. L. Robust colorimetric assays for dynamin's basal and stimulated GTPase activities. *Methods Enzymol* **404**, 490-503, doi:10.1016/s0076-6879(05)04043-7 (2005).

51 Zheng, S. Q. *et al.* MotionCor2: anisotropic correction of beam-induced motion for improved cryo-electron microscopy. *Nat Methods* **14**, 331-332, doi:10.1038/nmeth.4193 (2017).

52 Rohou, A. & Grigorieff, N. CTFFIND4: Fast and accurate defocus estimation from electron micrographs. *J Struct Biol* **192**, 216-221, doi:10.1016/j.jsb.2015.08.008 (2015).

53 Diaz, R., Rice, W. J. & Stokes, D. L. Fourier-Bessel reconstruction of helical assemblies. *Methods Enzymol* **482**, 131-165, doi:10.1016/s0076-6879(10)82005-1 (2010).

54 Schindelin, J. *et al.* Fiji: an open-source platform for biological-image analysis. *Nature Methods* **9**, 676-682, doi:10.1038/nmeth.2019 (2012).

55 Esterozi, L.

56 Sanchez-Garcia, R. *et al.* DeepEMhancer: a deep learning solution for cryo-EM volume post-processing. *Communications Biology* **4**, 874, doi:10.1038/s42003-021-02399-1 (2021).

57 Collaborative data science Publisher: Plotly Technologies Inc. (Montréal, QC 2015).

58 Jumper, J. *et al.* Highly accurate protein structure prediction with AlphaFold. *Nature* **596**, 583-589, doi:10.1038/s41586-021-03819-2 (2021).

59 Williams, C. J. *et al.* MolProbity: More and better reference data for improved all-atom structure validation. *Protein Sci* **27**, 293-315, doi:10.1002/pro.3330 (2018).
60 Adams, P. D. *et al.* PHENIX: a comprehensive Python-based system for macromolecular structure solution. *Acta Crystallogr D Biol Crystallogr* **66**, 213-221, doi:10.1107/s0907444909052925 (2010).

Data and code availability

Structural data supporting findings in this study have been deposited in the Protein Data Bank (PDB) and the Electron Microscopy Data Bank (EMDB). The accession codes of the cryo-EM maps and accompanying atomic models have been provided for: (1) sOPA1 (EMDB-xxxxx, PDB:xxx): (2) sOPA1 (EMDB-xxxxx, PDB:xxx)

Acknowledgments

This work was supported by the NIDDK and NHLBI NIH Intramural Research Program. This work used the NIH Multi-Institute CryoEM Facility (MICEF) and the NIDDK CryoEM core facility, NHLBI light microscopy core facility, and the computational resources of the NIH HPC Biowulf cluster (http://hpc.nih.gov). We would like to thank David Nyenhuis, John A. Hammer, Huaibin Wang, Yanxiang Cui, Haotian Lei, Andy Kehr, and Hank Breen for technical support with the cellular biology, electron microscopy, and computing.

Author contributions

S.B.N. and J.E.H. designed the research. S.B.N. and A.E.S. prepared protein samples. A.E.S. performed the GTPase assay. SBN collected cryo-EM data. S.B.N., B.C. and J.E.H. processed and analyzed the data. S.B.N. and X.W. designed and performed cell-based assays. M.P.S. and S.B.N. generated all constructs for cell-based assays. Y.Y. grew and maintained cells for cell-based assays. S.B.N. and J.E.H. wrote the paper. All authors were asked to comment on the manuscript.

Supplementary Files

This is a list of supplementary files associated with this preprint. Click to download.

- Nyenhuismovie1.mp4
- Nyenhuismovie2.mp4